A TWO-DIMENSIONAL MICROFLUIDIC SEPARATION PLATFORM FOR HIGH-THROUGHPUT GENETIC MUTATIONAL ANALYSIS

By

Jesse Stephen Buch

Thesis submitted to the Faculty of the Graduate School of the
University of Maryland, College Park in partial fulfillment
of the requirements for the degree of
Doctor of Philosophy
2003

Advisory Committee:

Professor Cheng S. Lee, Chair
Professor Dorothy Beckett
Professor Douglas English
Professor Catherine Fenselau
Professor Stephen Mount

PREFACE

Chapters two and three in this dissertation were co-authored and previously submitted for publication. Copyright permissions for the reproduced manuscripts were obtained from the publishers and are indicated on the first page of both chapters. Furthermore, the inclusion of reproduced manuscripts in this dissertation is permitted by the Department of Chemistry and Biochemistry and the Graduate School at the University of Maryland, College Park.

In the cases for both manuscripts, I was the primary author. In addition to my own written work, contributions from the coauthors named to the manuscripts constituting chapters two and three of this thesis consisted solely of critiques and suggested revisions received from my dissertation advisor, Dr. Cheng S. Lee. All other persons named as coauthors were recognized exclusively for contributions made to the work that is reported in the manuscripts.

DEDICATION

To Mom, Dad, Ethan, and Aron,

You have always been there to support me in every endeavor I have undertaken. I can never thank you enough.

To Nancy,

You have stuck by my side in thick and thin throughout this entire process. I could not have finished without you.

ACKNOWLEDGEMENTS

I would like to thank Dr. Pen-Chang Wang for his help with the work presented in Chapter 2. Fred Rosenberger and Yan Li provided an immense amount of fabrication support in fabricating a substantial portion of the silicon templates and microfluidic devices that were used in the studies presented in Chapter 3 and Chapter 4. For their help, I am extremely grateful. Christopher Kimball is gratefully acknowledged for his work with integrated microheaters and sensors that enabled the development and demonstration of the integrated spatial TGGE device presented in Chapter 3. I would like to thank Edd Cole for providing invaluable instruction and assistance with the manufacturing and machining of the custom hardware required for the work outlined in this dissertation. Dr. Ed Highsmith and Dr. Caren Chang are also gratefully acknowledged for their assistance in generating the DNA samples required for the studies presented in Chapter 3 and Chapter 4. Finally, I would like to acknowledge my advisor, Dr. Cheng S. Lee, for his tutelage during the course of my studies for the doctor of philosophy degree.

The financial support for this work by the National Cancer Institute (through Grants R21CA83871 and CA092819) and the Analytical Chemistry Division of the National Institute of Standards and Technology are gratefully acknowledged.

TABLE OF CONTENTS

LIST OF TABLES

LIST OF FIGURES

CHAPTER ONE

INTRODUCTION

The fundamental and complex biochemical processes that sustain life in the human body are ultimately governed by the elemental genetic information that defines the physical nature of all human beings. This genetic information is encoded in the form of deoxyribonucleic acid (DNA) molecules situated in the nuclei of constituent cells of the body and is collectively denoted as the human genome.

As the human genome provides the elementary blueprint for all innate processes that sustain life in the human body, increasing our understanding of the structure and function of the human genome has remained of utmost importance. Consequently, scientists worldwide have worked toward mapping and sequencing the entire human genome over the past two decades. This massive collective effort has been dubbed The Human Genome Project (HGP).

It has long been understood that various diseases and disorders can be linked to defects or mutations within well-defined loci of the human genome known as genes. As a result, the nature and location of these mutations and their relationship to associated genes and gene function has been the subject of lengthy and in-depth

study. For example, sickle cell anemia has been linked to a single base mutation (adenine to thymine substitution at the second position of the sixth codon) in the β-globin gene [1]. In addition, assorted mutations occurring in the p53 tumor suppressor gene (~90% of which occur in exons 5-8) have been associated with numerous cancers. The presence of germline, or inherited mutations in the p53 gene causes Li-Faumani syndrome, which is characterized by greatly increased risks of a variety of cancers and the occurrence of multiple cancers in a single individual [2].

The Human Genome Project has provided scientists with an unprecedented wealth of information as new genes are being discovered at an accelerated rate along with the determination of the function of these genes (functional genomics). With the first draft of the genome completed, a reference is now available against which all sequencing data can be compared. As a result, the increased ability to correlate specific genes, or mutations within these genes, with particular disease states has produced an assortment of new genetic markers for use in diagnosing and predicting genetic-based diseases. Employment of this newly acquired cache of genomic data has been primarily directed toward improving disease prevention and disease management, with cancer and genetic disorders serving as the principal targets [3].

Major emphasis has been placed upon the enhancement of medical technology, which is expected to ultimately result in superior and more personalized health care for all. Advances in analytical technology and genetic understanding have resulted in improved medical diagnostics, for earlier disease detection and

more accurate disease prognosis. Likewise, recent innovations are also paving the way for new therapies that possess potential for providing more effective treatment of genetic-based disease. The importance placed on such endeavors is no better illustrated than by the immense public attention currently paid to the field of gene therapy even as it remains in its infancy. Ultimately, significant improvement in our abilities to diagnose, prognosticate, and treat disease is critical to enhancing the quality and longevity of human life worldwide.

TRADITIONAL METHODS OF GENETIC MUTATION DETECTION

A primary challenge to augmenting genetic-based disease prevention and management is the establishment of new analytical strategies for detecting genetic mutations that surpass the performance and capabilities of traditional gel-based approaches. The need to screen individuals for the presence of sequence heterogeneity across a large number of genes requires the development of technology that can more rapidly, more accurately, and more cost-effectively identify DNA sequence heterogeneity.

Currently, nucleotide sequencing remains the "gold standard" for mutational analyses as it provides the most reliable method for accurately detecting and fully characterizing mutations [4-6]. However, the high cost and expenditure of time associated with contemporary sequencing technology, as well as the difficulties that hinder sequencing in detecting heterozygous mutations, make alternative approaches more attractive in many cases. Furthermore, mutations occur in the genome at a rather low frequency. A recent estimate asserts the presence of 2.1 million single nucleotide polymorphisms (SNPs) in the human genome occurring at

a density of approximately 1 per 1,250 bases of sequence [7]. This estimate further maintains the position of nucleotide sequencing as a comparatively inefficient approach to the large-scale investigation of genomic sequence heterogeneity, especially in large population-based screening. As a result, various approaches have been developed to provide more cost-effective pre-screening of mutations in relatively large pieces of DNA. Alternative prescreening techniques include single-strand conformation polymorphism (SSCP) analyses [8,9], hybridization analyses [10-12], and heteroduplex-based analyses such as denaturing gradient gel electrophoresis (DGGE) [13-15].

Mutational analysis by single-strand conformation polymorphism (SSCP) is one of the most popular methods employed in the field. In SSCP, double-stranded DNA fragments are first denatured. The resulting single-stranded fragments take on tertiary structures similar to RNA with their electrophoretic mobilities dependent on the resulting conformations. Because mutant strands will have a different conformation than that of the wild-type strands, they are detected when more than one band appears on the gel for a given sized fragment. While simple and inexpensive to perform, SSCP suffers from poor sensitivity and the failure to accurately analyze single-stranded sequences greater than 200 base pairs [3,16].

Hybridization analysis is a method that has become increasingly popular due to its implementation in microfluidic devices, referred to as “DNA microarray chips”, which have recently become commercially available. In hybridization analyses performed on a DNA chip [9,10], 20-25-mer oligonucleotide probes matching all of

the possible single-nucleotide substitutions for a gene are synthesized and immobilized on the microchip substrate to form an oligonucleotide array. A solution of PCR-amplified and fluorescently labeled DNA containing the gene or gene segment of interest is transported into the hybridization chamber and allowed to incubate over a lengthy time interval. The DNA solution is then removed, unbound probes are washed away, and the immobilized probes are illuminated by an excitation light source. When illuminated, spots on the chip where hybridization has occurred emit fluorescence indicating the presence of a mutation.

Although this developing technology is quite promising, it is presently hindered by high costs. Moreover, these chips can only be used to screen a very limited range of genes, as the sequence of the gene of interest must be extensively verified to provide the required hybridization probes. DNA microarray chips also suffer from lengthy analysis times due to their reliance upon diffusion kinetics during the hybridization step. Admittedly, the number of spots that can be packed into a small region on the chip is enormous. However, one must routinely employ numerous spots to span a mismatch and utilize multiple chips for large and composite gene testing [17].

Additional screening techniques employ the formation of heteroduplexes to reveal differentiation between two sequences. Since most mutations occur in heterozygous form (i.e. in one allele), heteroduplexes can be formed from polymerase chain-reaction (PCR) products by denaturing them before allowing them to slowly re-anneal. In the case of homozygous mutations, the addition of

reference wild-type DNA, such as cDNA containing the consensus sequence of interest, is necessary. The presence of heteroduplexes can then be revealed by differences in the average electrophoretic mobilities of the duplexes due to differential denaturing/melting temperature profiles. DGGE is arguably the most significant of the heteroduplex-based mutation screening techniques. It is performed on a denaturing gradient gel with urea or formamide serving as the denaturing reagent. Because mutations almost always disrupt and weaken the base pairing of double-stranded DNA regions in which they are present, mutated DNA will denature at a lower concentration of denaturing reagent. Since the electrophoretic mobility of a molecule is related to its conformation, DNA fragments of the same size, but of different sequence, can be distinguished due to dissimilar rates of denaturation while being transported through a gel by electrophoresis. The denaturing gradient induces lower average electrophoretic mobilities during the separation for the fragments containing weaker base-pairing sequences. One advantage provided by DGGE is that it can be used to screen both known and unknown genes depending on whether specific or non-specific PCR is used to produce the heteroduplexes. Furthermore, once optimized DGGE provides excellent sensitivity for known and unknown mutations. An analogous technique to DGGE is temperature gradient gel electrophoresis (TGGE) [16]. TGGE employs the same separation mechanism as DGGE but instead induces DNA denaturation by establishing a temporal or spatial temperature gradient through controlled heating of the gel.

TWO-DIMENSIONAL GENE SCANNING

A strategy for increasing the resolving power and throughput of genetic mutational analyses is to employ multidimensional separations in series. Fischer and Lerman [19] first introduced two-dimensional (2-D) DGGE as an example of such a strategy. In demonstrating the immense resolving power of such an approach, Fischer and Lerman succeeded in utilizing 2-D DGGE to resolve the entire *E. coli* genome in two dimensions and detect sequence heterogeneities [19]. Aside from nucleotide sequencing, 2-D DGGE is the only method which provides nearly 100% sensitivity for mutation detection. Assuming the sequence of the fragment of interest is known, DGGE can be simulated on the basis of melting point theory using a computer-run algorithm. Furthermore, a GC-rich fragment (GC clamp) can be attached to one of the PCR primers. Because poly-GC regions exhibit the strongest base pairing, this enables a target fragment to be designed so that it will always be the lowest melting domain, providing the utmost sensitivity for all types of mutations.

The capability to perform multidimensional separations such as 2-D DGGE provides analytical support for utilizing more complex sample preparation strategies such as PCR multiplexing. Under optimized conditions, as many as 10 or more PCR reactions can be carried out in a multiplex fashion within the same reaction volume [20]. Due to the parallel sample processing involved, multiplex PCR essentially normalizes much of the variability involved in preparing individual PCR reactions such as pipetting accuracy and individual PCR reaction variability.

Additional advantages to performing multiplex PCR include reduced sample preparation time and thus an increase in information obtained per unit time. Also, the ability to perform several reactions in the same volume significantly reduces the amount of reagents required, especially with regards to the amount of template required.

Through the incorporation of extensive PCR multiplexing with 2-D DGGE, Vijg et al. [21,22] have succeeded in greatly improving upon the capacity and resolving power of 2-D DGGE. Dubbed two-dimensional gene scanning (TDGS) by its founders, this scheme provides a platform for performing parallel analyses of mutational variants in multiple genes. The exceptional resolving capability of TDGS in the slab gel format has been demonstrated for several large human disease genes, including BRCA1 (breast and ovarian cancer susceptibility gene 1) [22], CFTR (cystic fibrosis transmembrane regulator gene) [23], RB1 (retinoblastoma tumor suppressor gene)[24], MLH1 (MutL protein homolog 1) [25,26], and TP53 (*p*53 tumor suppressor gene) [27]. TDGS has also been utilized in analyzing a portion of the mitochondrial genome [28].

In order for a gene-scanning method to be amenable to large-scale analysis of a broad range of human genes in large population-based studies, it must provide accurate detection in combination with a facility for operating at a high throughput and cost-effective manner. In its current state, TDGS succeeds in being relatively cost-effective when weighed against other mutation detection techniques [22]. However, TDGS has yet to be implemented in a high-throughput platform for

comprehensive DNA analysis. Despite the selectivity and sensitivity provided by traditional TDGS, this technique as carried out today is a compilation of manually demanding and time-consuming tasks, susceptible to irreproducibility and inferior quantitative accuracy.

MICROFLUIDICS

The search for increasingly higher throughput analysis platforms has been a primary focus of Analytical chemists beyond the past decade. One upshot of this focus has been the rapidly emerging field of microfluidics technology [29-34]. Microfluidics improves upon existing analytical diagnostic platforms due to the amenability of the technology towards miniaturization, automation, analysis speed, and fabrication, all of which are critical aspects associated with the development of high throughput platforms. Microfluidics also provides the advantages of durability and minimal sample consumption. With the benefits provided by microfluidics, a substantial movement exists toward implementing contemporary genetic mutational analysis technologies in microfluidic platforms. Currently, the majority of microfluidic devices developed for genomic analysis consist of simple platforms, which merely embody existing techniques, such as sequencing [35,36], conventional heteroduplex analysis [37], and SSCP [38], in a miniaturized format. However, the true power of microfluidic technology lies in its unparalleled ability to perform high-throughput and multi-dimensional analyses without sacrificing efficiency and resolution. Thus, the need exists for the development of more complex devices that will be able to harness and exploit this inherent capability.

Over the past decade, the search for materials that are compatible with microfluidic technology has produced a dichotomy in the field. At one end of the spectrum lie devices fabricated from glass or silicon [29-38]. These materials are attractive in that they tend to have uniform and well-characterized surface properties, which are important in electroosmosis-driven microfluidic operations. Furthermore, techniques and methodologies including various surface coatings and treatments previously developed for capillaries are readily transferable to these platforms. In the case of glass, the optical properties are suitable for sensitive optical detection as well. The processes involved in fabricating microchips from glass and silicon, however, are not amenable to mass-production. As a result, glass and silicon microchips can be relatively expensive. This has led to the search for viable plastic materials that can be used as substrates for fabricating functional microfluidic platforms.

To date, plastics have proven disadvantageous to glass when considering the autofluorescence and lack of surface property understanding associated with them. However, they are highly attractive due to their amenability toward fabrication methods that can mass-produce these devices. The impetus behind the push to produce viable plastic microfluidic devices is the ultimate goal of developing inexpensive, disposable devices that can eliminate cross-contamination between separate analyses [37]. Of the plastics that have been investigated for this purpose, three have emerged at the forefront. Polydimethylsiloxane (PDMS) [38,39], polymethlymethacrylate (PMMA) [40,41], and polycarbonate (PC) [42]

have all been utilized to fabricate functional microfluidic devices that have been employed in numerous analytical and bioanalytical applications.

2D MICROFLUIDIC SEPARATIONS FOR MUTATION ANALYSIS

When considering the advantages afforded by microfluidics, the obvious strategy for increasing the throughput and cost-effectiveness of TDGS is to implement the technology in a microfluidic platform. Thus, the design, development, and characterization of a novel polymer 2-D microfluidic separation platform have been investigated. Briefly, the entire microfluidic channel network is filled with an electrophoretic size-sieving matrix. Using the gated valve injection technique, a mixture of PCR amplicons are injected into a single, first-dimension separation channel and separated by size via gel electrophoresis. The size-resolved amplicons are then electrokinetically and quantitatively transferred into a second separation dimension, which consists of an array of orthogonal channels all of which intersect with the first dimension channel at evenly distributed intervals. Following the electrokinetic transfer of the analyte bands, each amplicon is examined for sequence heterogeneity via separation by TGGE. Fluorescence in each channel of the second dimension array is simultaneously detected with a CCD camera by laser-induced fluorescence detection.

PROJECT DESCRIPTION

The development of fabrication methods for polymeric microfluidic separation platforms and the application of these first generation devices to performing direct

manipulation of electroosmotic flow is outlined in Chapter two. In this work, the amenability of a simple polydimthylsiloxane-based polymeric microfluidic system toward field-effect electroosmotic flow control was investigated.

The microfluidic system consisted of a 2.0 cm open microchannel fabricated on a PDMS slab, which can reversibly adhere to a silicon wafer to form a hybrid microfluidic device. Aside from mechanically serving as a robust bottom substrate to seal the channel and support the microfluidic system, the silicon wafer was exploited to achieve field-effect flow control by grounding the semi-conductive silicon medium. When an electric field was applied through the channel, a radial electric potential gradient was generated across the silicon dioxide layer to allow for direct control of the zeta (ζ) potential and the resulting electroosmotic flow (EOF). By configuring this microfluidic system with two power supplies at both ends of the microchannel, the applied electric potentials could be varied for manipulation of the polarity and magnitude of the radial electric potential gradient across the silicon dioxide layer. At the same time, the longitudinal potential gradient through the microchannel, used to induce EOF, was held constant.

The results of EOF control in this hybrid microfluidic system are presented for phosphate buffer at pH 3 and pH 5. EOF control achieved at higher solution pHs of 6 and 7.4 by modifying the microchannel surface with cetyltrimethylammonium bromide (CTAB) is also presented. Results of EOF control from this study are compared with those reported in the literature involving the use of fused-silica capillary systems and microfluidic devices under comparable conditions.

Chapter three illustrates the technical basis and demonstration of a miniaturized system for DNA mutation analysis, utilizing temperature gradient gel electrophoresis (TGGE) in a polycarbonate (PC) microfluidic device. Bulk heater assemblies were designed and employed to externally generate temperature gradients in spatial and temporal formats along the separation channels. TGGE analyses of model mutant DNA fragments, each containing a single base substitution, successfully revealed the presence of sequence heterogeneity in each model heteroduplex sample. Results were achieved using both single and 10-channel parallel measurements in a microfluidic platform.

Additionally, a comprehensive polymer microfluidic device containing an integrated microheater and sensor array was developed and demonstrated for performing spatial TGGE for DNA mutation analysis. The device consisted of two PC modular substrates mechanically bonded together. One substrate was embossed with microchannels while the other contained a tapered microheater, lithographically patterned along with an array of temperature sensors. Compared with the external heating approaches, the integrated platform provided significant reduction in power requirement and thermal response time while establishing more accurate and highly effective control of the temperature gradient for achieving improved separation resolution.

The conception and realization of a parallel two-dimensional microfluidic platform for genetic mutation screening is described in Chapter four. A microfluidic system was designed and fabricated to include an imprinted two-

dimensional network of microchannels in a PC substrate. The first separation dimension on the platform consisted of a single channel for performing size-based gel electrophoresis on a mixture of PCR products. Due to the discontinuous sidewalls of the first dimension separation channel, extensive finite element modeling (FEM) was performed to optimize controllable geometric factors at the interface between the first dimension and second dimension channels. This was done to minimize analyte band dispersion caused by the side channel junctions along the first dimension channel as well as the electrokinetic transfer process from the first separation dimension to the second. The second separation on the platform involved an array of ten microchannels in which each PCR product resolved by size in the first dimension was interrogated for the presence of sequence heterogeneity individually with parallel microfluidic TGGE. The comprehensive two-dimensional mutation analysis performed using this microfluidic system demonstrated the capability to detect mutations in DNA fragments at speeds approximately one to two orders of magnitude higher than is possible with conventional gel-based TDGS.

Ultimately, the novel aspects of this work include the development of a multidimensional microfluidic separation system that is capable of performing high throughput analyses in parallel. For the first time, TGGE was successfully demonstrated in a microfluidic format in both single and parallel modes. The ability to resolve sequence variants using both temporal and spatial thermal gradients was also verified. Implementing the TDGS process in a miniaturized platform enables

mutation analyses to be performed at speeds unparalleled by competitive approaches.

CHAPTER TWO

Field-Effect Flow Control in a Polydimethylsiloxane-Based Microfluidic System

INTRODUCTION

The microfluidic device is rapidly supplanting capillaries as the platform of choice for performing electrokinetic separations and biochemical analyses. The advantages of such analytical microsystems include automation, efficiency, integration, minimal sample consumption, and speed [39-41]. The majority of microfluidics work has involved the fabrication of glass and silicon-based chips [42-44]. However, the widespread interest in microfluidic devices for bioanalytical applications has resulted in efforts to facilitate the use, and to reduce the cost, of such devices. As a result, polymeric materials such as PDMS and polymethyl methacrylate have been explored as more versatile alternatives for the fabrication of microfluidic devices [45-50].

As the pumping mechanism of choice in microfluidic network [51,52], electroosmosis provides several advantages over micro-machined pressure driven pumps, including ease of fabrication and the absence of moving parts. Moreover, sample plugs suffer little from dispersion in electroosmotic pumping due to the nearly uniform fluid velocity profile across the channel diameter. EOF is generally controlled by manipulating the chemical composition of the buffer solution (i.e. buffer additives, ionic strength, organic content, and solution pH), or by coating of the inner wall of the fluid channel. However, these chemical methods do not allow for the dynamic regulation of EOF.

A physical means for effective control of EOF, involving the application of an external radial electric field, has been demonstrated in fused-silica capillaries [53-56] and, more recently, in microfluidic devices [57,58]. The ability to physically manipulate EOF is advantageous as it allows for dynamic flow control at any point during either the mobilization or separation of analytes in an electrophoresis experiment. Such capability also provides spatial control of EOF at points of interest within the microfluidic network.

In this work, a hybrid microfluidic device is constructed for low-voltage studies of field-effect flow control at various solution conditions. The device consists of a 2-cm long microchannel fabricated on a PDMS substrate. The channel is reversibly sealed using a silicon wafer coated with a 2.0 μm thick silicon dioxide layer. The field-effect for direct control of electroosmosis is obtained by grounding

the backside of silicon wafer for the creation of a radial electric potential gradient across the silicon dioxide layer.

EOF control results are compared with those reported using fused-silica capillary systems [53,59,60] and microfluidic device [57,58]. Due to the application of thin insulating layers for comprising fluid channel walls, the absolute magnitude of radial electric voltages required for achieving EOF control is about two (across 2 μm silicon dioxide in this study) to three [57] (across 0.4 μm silicon nitride) orders of magnitude lower than those applied across 50-150 μm-thick fused-silica [53,59,60]. Thus, the range of applied radial electric potential gradients (radial electric potential/thickness of channel wall) for achieving field-effect flow control measured in this study is in agreement with those reported using fused-silica capillaries [53,59,60] and a silicon nitride microfluidic network [57]. However, Polson and Hayes have reported enhanced EOF control while applying radial electric potentials in the low-voltage range across 50-μm thick glass walls. The source and mechanism responsible for the enhanced EOF control in the studies of Polson and Hayes [58] are unclear.

EXPERIMENTAL SECTION

Materials and Reagents. 4" <100> oriented p-type silicon wafers containing 2.4 μm silicon dioxide coating were obtained from WaferNet, Inc. (San Jose, CA) and were used for the template fabrication. 4" <100> oriented p-type silicon wafers coated with a 2.0 μm thick silicon dioxide layer were acquired from Nova

Electronics Materials (Richardson, TX) and were employed for the construction of hybrid microfluidic devices. CTAB and sodium mono- and diphosphate were purchased from Sigma (St. Louis, MO). The Sylgard® 184 PDMS kit was obtained from Dow Corning (Midland, MI). All solutions were prepared using water purified by a SYBRON/Barnstead Nanopure II system (Boston, MA) and further filtered with a 0.22 μm membrane (Costar, Cambridge, MA)

Fabrication of Silicon Template. The fabrication of a silicon template was performed by following standard procedures involving photolithography and chemical etching. First, the 2.4 μm-thick silicon dioxide surface of the <100> oriented p-type silicon wafer was covered by a layer of photoresist. Then, a patterned photomask, which consisted of the channel design printed with high resolution onto a transparency, was placed on top of the photoresist layer.

Following the exposure of the wafer to ultra-violet light, the photoresist was developed to form the desired patterns and features on the wafer surface. The wafer was then etched with buffered hydrofluoric acid solution to remove the silicon dioxide except for that under the protection of the developed photoresist. The remaining silicon dioxide pattern acted as a protection mask so that the silicon could be etched anisotropically in 30% (w/v) potassium hydroxide solution to form a positive relief mold containing the desired three-dimensional structures for the fabrication of PDMS microchannels.

Fabrication of PDMS Microchannel and Assembly of Hybrid Microfluidic Device. The PDMS base and curing agent were mixed 10:1 (v/v) and poured over the silicon template, which was fixed in a large petri dish. The template provided a positive relief mold for the formation of the channel in the PDMS substrate. The PDMS was allowed to cure at room temperature for 3 days in a ventilation hood. After curing, the 1-cm thick PDMS slab was carefully removed from the template and holes (0.5 cm in diameter) were punched at each end of the channel to provide access from the reservoirs to the channel.

Reservoirs were constructed by taking two square pieces of PDMS (2 cm on each side) and removing a circular portion (1.5 cm in diameter) from the center. The reservoirs were placed on the topside of the substrate and the channel along the bottom side of the substrate was sealed by a silicon wafer coated with a 2.0 μm thick silicon dioxide layer (see Fig. 2.1). An airtight seal was gained by this simple stacking due to the adhesive nature of PDMS. The silica dioxide layer on the underside of the silicon wafer was scratched away to provide access to the semi-conductive silicon medium of the wafer. The entire underside of the upper silicon dioxide layer, which served as the bottom surface of the microchannel, was grounded through the silicon medium by attaching a grounding wire with conductive epoxy (Chemtronics, Kennesaw, GA).

Current-Monitoring of Electroosmotic Flow. Two Spellman CZE 1000R high voltage power supplies were employed to apply various electric potentials at

both ends of the microchannel through platinum electrodes in the solution reservoirs. Because most high voltage power supplies are not designed to operate as current sinks, a 375 MΩ resistor was incorporated in parallel with the high voltage power supply connected to the outlet reservoir (see Fig. 2.2). The changes in EOF under influence of the field-effect were measured using the current monitoring method [60].

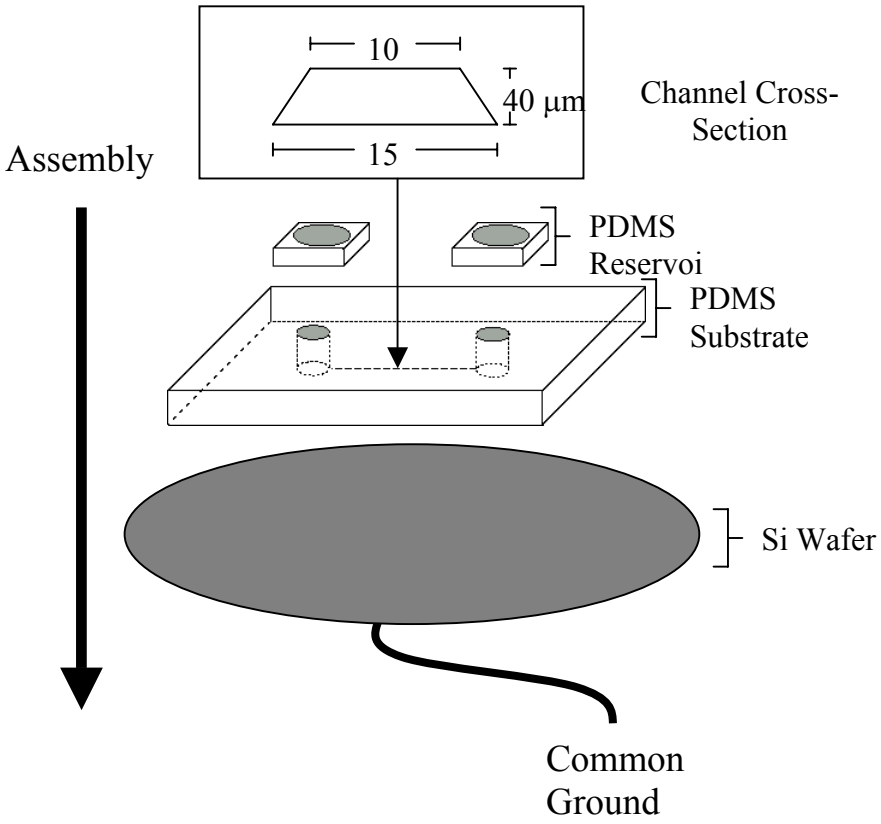

Figure 2.1 The components and assembly of the PDMS-based microfluidic system. The silicon wafer provides 44% of channel surface coverage for field-effect flow control.

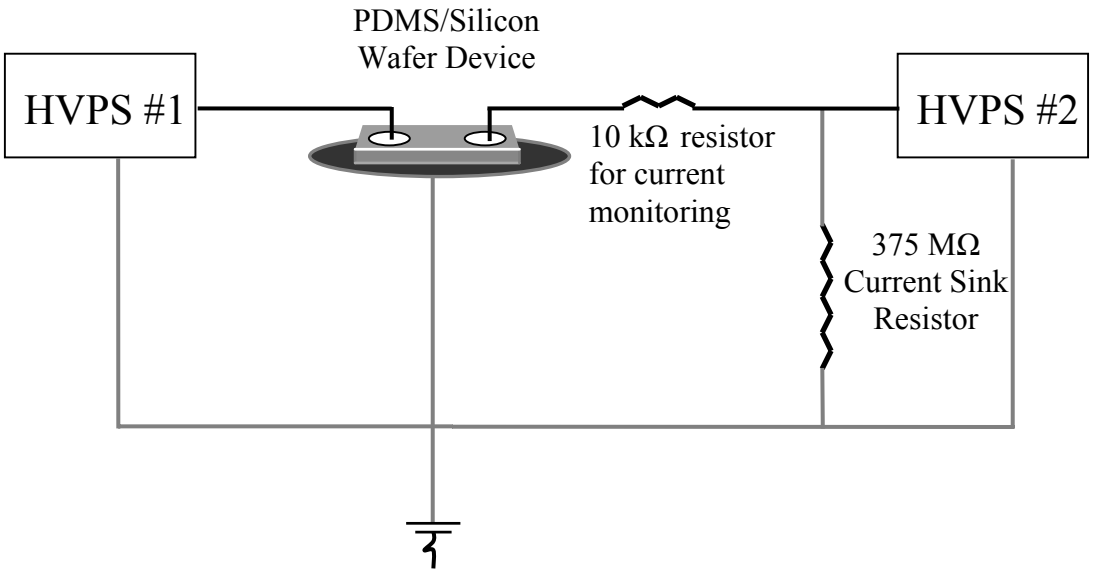

Figure 2.2 The electric circuit employed for the studies of field-effect flow control in a hybrid PDMS/silicon wafer device.

The current in the microchannel was measured by monitoring the voltage drop across a 10-kΩ resistor connected to the electrode in the outlet reservoir (see Fig. 2.2). In all runs, the channel was pre-filled with 1 mM phosphate buffer by vacuum. Both reservoirs were filled with 400 μL of 1 mM phosphate buffer and the current was monitored for one minute to verify stability. The 1 mM buffer in the reservoir at the high voltage end was then replaced with 3 mM buffer. As soon as the electric potentials were applied, the higher concentration phosphate buffer migrated into the

channel by electroosmotic pumping and increased the current in the circuit. Complete filling of the channel with the 3 mM phosphate buffer was indicated by a plateau in the current. The channel length divided by the time required to complete the filling process gave the rate of EOF.

Partial Modification of Channel Surface with CTAB. The silicon dioxide surface of the channel was modified with CTAB by incubating the silicon wafer substrate, prior to system assembly, with phosphate buffer containing 0.01 mg/ml CTAB for one hour. The wafer was then rinsed with deionized water, to remove any excess, unbound CTAB from the surface, prior to the assembly of the PDMS/silicon wafer hybrid device.

RESULTS AND DISCUSSION

Two separate electric voltages were applied at the inlet and the outlet reservoirs for inducing the EOF in the microchannel and creating various radial electric potential gradients across a 2.0 μm thick silicon dioxide layer in an effort to directly control the EOF. For example, an electric field strength of 150 V/cm in a 2-cm long microchannel was established by applying two individual voltages of 450 V and 150 V at the inlet and the outlet reservoirs, respectively. The voltages inside the channel, relative to a common ground on the back side of the silicon wafer, established the radial electric potential gradients which ranged from –2.25 MV/cm (0 – 450 V/2.0 μm) at the inlet end of the channel to -0.75 MV/cm at the channel

outlet. Thus, an average radial electric potential gradient of –1.50 MV/cm was simultaneously imposed for studying field-effect flow control.

Field-Effect Flow Control at Low pHs. By adjusting the applied electric potentials in the inlet and outlet reservoirs, we were able to maintain a constant electric field strength of 150 V/cm in the microchannel, while varying the polarity and the magnitude of average radial electric potential gradients across the insulating silicon dioxide layer for direct control of EOF. As shown in Fig. 2.3, application of negative radial electric potential gradients increased the electroosmotic mobility at pH 3 from 1.5 x 10^{-4} cm^2/V-s at 0 MV/cm to 2.9 x 10^{-4} cm^2/V-s at -1.5 MV/cm. By applying opposite polarity in radial electric potential gradients, the electroosmotic mobility was decreased to zero and eventually reversed at 2.3 MV/cm. The extent of EOF control decreased with increasing solution pH from 3 to 5. Such pH dependence of field-effect flow control was in good agreement with those reported in fused-silica capillary systems [53,59,60] and microfluidic devices [57].

Field-Effect Flow Control at Higher pHs Assisted by CTAB Surface Modification. The effectiveness of EOF control decreases at higher solution pHs because of the larger intrinsic surface charge and the higher capacitance of the electrostatic diffuse layer at the wall/solution interface. To demonstrate the ability to perform field-effect flow control at higher solution pHs, the silicon dioxide surface of the channel was coated with the EOF modifier CTAB. CTAB reduces

the ζ potential and enables us to manipulate the ζ potential at pHs where the ζ potential is normally too high to be significantly influenced via the field-effect. As shown in Figure 2.4, direct control of EOF was resumed at pH 6 and 7.4 by increasing the point of zero charge on the silicon dioxide surface.

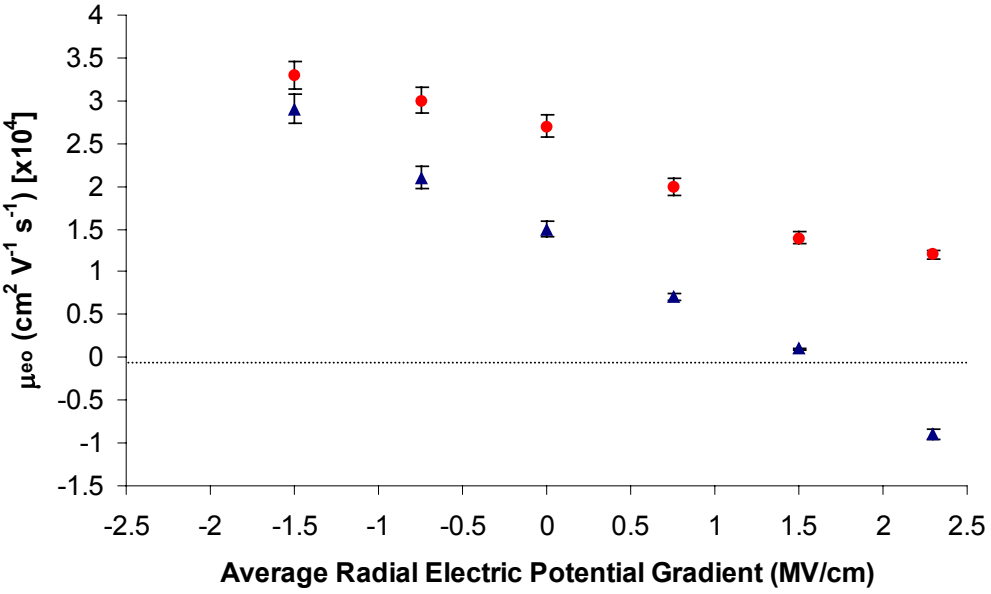

Figure 2.3 A plot of electroosmotic mobility vs. average radial electric potential gradient in pH 3 (▲) and pH 5 (●) phosphate buffers. The dashed line indicates the point of zero flow.

Surface Coverage of Microchannel Under Field-Effect. An important factor influencing the degree of field-effect flow control is the extent of the channel surface over which the ζ potential can be manipulated. The potassium hydroxide-

etching process involved in the fabrication of the silicon template produces a positive channel image with a trapezoidal cross section. This results in a trapezoid-shaped microchannel upon molding of the PDMS slab on the template. The dimensions of open PDMS microchannel (see Fig. 2.1) are as follows: 2.0 cm long; 40 μm deep; 103 μm wide at the top; and 155 μm wide at the bottom (facing the silicon wafer).

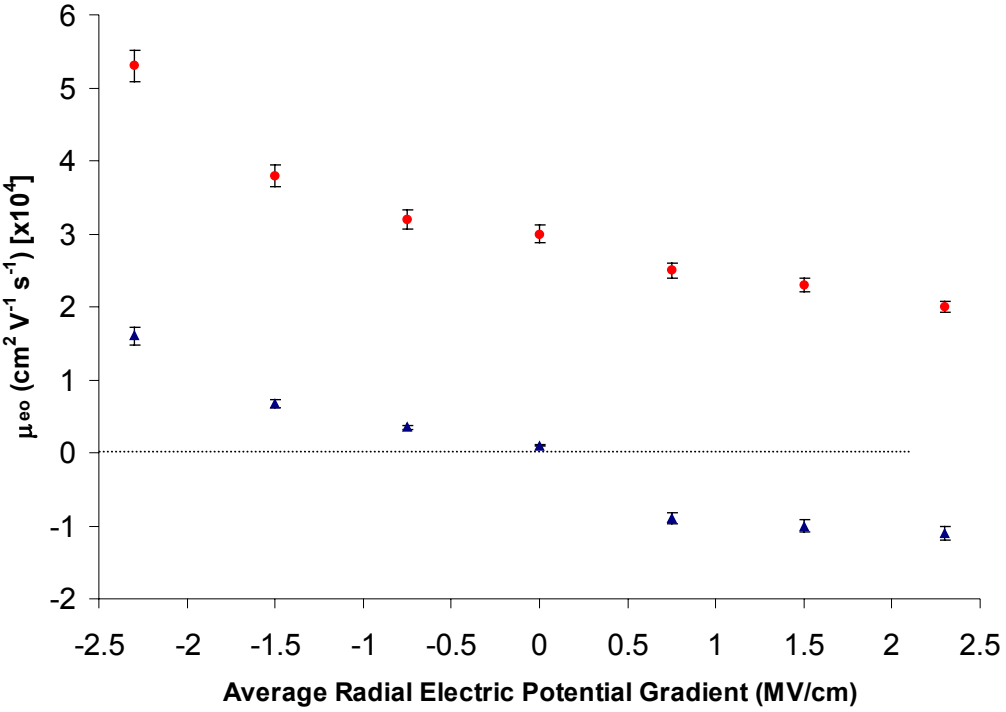

Figure 2.4 A plot of electroosmotic mobility vs. average radial electric potential gradient in pH 6 (▲) and pH 7.4 (●) phosphate buffers. The silicon dioxide surface of the channel is coated with CTAB to reduce its surface charge density.

Because the field-effect is only applied across the silicon dioxide surface of the channel, the trapezoidal shape provides us with 44% of channel surface under direct control of the ζ potential.

The electroosmotic mobility in molded PDMS microchannels [49] ranged from 0.15 x 10^{-4} cm^2/V-s at pH 3 to 4.0 x 10^{-4} cm^2/V-s at pH 7. Thus, the EOF originating from the silicon dioxide surface under the influence of applied radial electric potential gradients was mostly in the same direction as that contributed by the PDMS walls. However, bi-directional flow could occur in this hybrid microfluidic device when the EOF, originating from the silicon dioxide surface, was reversed using the large and positive radial electric potential gradients (see Figs. 2.3 and 2.4). Such bi-directional flow, flow in opposite directions in the same channel, has been demonstrated by Barker and co-workers [62]. A positively derivatized plastic substrate with a negatively charged lid was used to achieve top-bottom opposite flows. Derivatization of the two sides of a plastic microchannel with oppositely charged polyelectrolytes was employed to establish side-by-side opposite flows.

Microfluidic Devices Versus Capillary Systems in Field-Effect Flow Control. EOF control results obtained from this study were compared with those reported in the literature using fused-silica capillary systems [53,59,60] and microfluidic devices [57,58] (see Table 2.1). The cylindrical capacitor factor [57,60], $1/(r_i \ln (r_o/r_i))$, was included for the calculation of the range of applied radial electric

potential gradient in fused-silica capillaries, where r_i and r_o are the inner and the outer radii of the capillaries, respectively. The percentage of total channel surface under the influence of the field-effect was also estimated from experimental details or figures in each study. For example, in the work of Polson and Hayes [58], two 6.0 mm-long external voltage electrodes were located parallel to and on either side of a 5-cm main channel separated by 50 μm of glass substrate. The percentage of field-effect coverage was therefore estimated to be around 12% in this particular system configuration.

The control factor summarized in Table 2.1 is simply calculated by determining the range of electroosmotic mobility under field-effect flow control and dividing it by the range of the applied radial electric potential gradient. Of the studies summarized in Table 2.1, the last three works involved the use of the field-effect for flow control in microfluidic systems. By taking into account both the control factor and the percentage of field-effect coverage, our studies and the work reported by Schasfoort et al. [57] displayed flow control on the same order of magnitude as those performed in capillary systems [53,59,60]. However, comparable flow control in both studies, involving the use of microfluidic devices, was achieved using radial electric potentials one to two orders of magnitude smaller than those applied in capillary systems.

The ability to effectively control the EOF in microfluidic devices is the result of using an extremely thin insulating layer (2.0 μm silicon dioxide in our study and 0.4 μm silicon nitride in the work of Schasfoort et al. [57]) as part of the channel

wall. Thus, comparable radial electric potential gradients can be attained for direct control of EOF by applying much lower radial electric potentials across extremely thin insulating layers. In contrast, it is not clear as to what the origin and the mechanism are that are responsible for the enhanced EOF control observed by

Table 2.1 Comparison of the Results Reported in This Study with Those Reported in the Literature[a]

pH	Buffer Ionic Strength (mM)	Thickness of capillary or channel wall (μm)	V_{rad} (V)[b]	E_{rad} (V/cm)[c]	$\Delta\mu_{eo}$ (cm^2/V-s)[d]	Control Factor ($\Delta\mu_{eo}/E_{rad}$)	Percent Coverage
Lee, McManigill, Wu, and Patel **[53]**							
5	1,2	75/375	11,000	1.8×10^{6}	3.0×10^{-4}	1.6×10^{-10}	85 %
Hayes, Kheterpal, and Ewing **[59]**							
3	1	10/144	20,000	1.5×10^{7}	6.4×10^{-4}	4.3×10^{-11}	80%
3	1	25/250	20,000	6.9×10^{6}	6.4×10^{-4}	9.2×10^{-11}	80%
5	1	25/250	20,000	6.9×10^{6}	3.1×10^{-4}	4.5×10^{-11}	80%
Huang, Tsai, Wu, and Lee **[60]**							
3	10	50/150	20,000	7.3×10^{6}	4.1×10^{-4}	5.6×10^{-11}	85 %
Schasfoort, Schlautmann, Hendrikse, and Van den Berg **[57]**							
3.6	2	0.4	52.5	1.6×10^{6}	3.4×10^{-4}	2.1×10^{-10}	45%
4.5	2	0.4	100	2.6×10^{6}	1.6×10^{-4}	6.2×10^{-11}	45%
Polson and Hayes **[58]**							
3	20	50	120	2.4×10^{4}	7.9×10^{-5}	3.3×10^{-9}	12%
Buch, Wang, and Lee							
3	1,3	2	750	3.8×10^{6}	3.8×10^{-4}	1.0×10^{-10}	44%
5	1,3	2	750	3.8×10^{6}	2.1×10^{-4}	5.5×10^{-11}	44%

a) Data from literature was calculated from experimental details or figures
b) Range of applied radial electric voltage
c) Range of applied radial electric potential gradient
d) Range of electroosmotic mobility achieved with field-effect flow control

Polson and Hayes [58]. In their studies, the control factor obtained from a surface coverage of only 12% was at least one order of magnitude greater than the rest of work summarized in Table 2.1. Furthermore, the range of their radial electric potential gradient, which was achieved by applying 120 V across 50 μm thick glass layer, was about two orders of magnitude lower than those reported in the literature [53,57,59,60] using capillary systems and microfluidic devices.

CONCLUSION

The realization of true lab-on-a-chip technology, in which the functionality of desktop biochemical analytical tools is replicated in a credit card sized package, will require flow control in complex microfluidic networks of interconnected channels between mixers, reactors, reservoirs, sensing elements, and related components. A hybrid microfluidic device is employed in this study for the demonstration of EOF control by directly manipulating the ζ potential at the interface through the use of the field-effect. The impact of the use of ultrathin insulating walls for the channels in microfluidic devices is that significantly smaller radial electric voltages are used to create the extraordinary fields required to have effective field-effect flow control.

In the work reported by Schasfoort et al. [57], silicon nitride is employed as the dielectric wall material, with a relative permittivity of approximately $\varepsilon_r = 6$ and a thickness of 0.4 μm. While silicon dioxide has a relative dielectric constant similar to that of nitride ($\varepsilon_r = 4$), it offers several important advantages compared to silicon nitride such as controllable thicknesses as small as 50 nm or lower, high dielectric

breakdown strength (20 MV/cm for thermal oxide), low film defect density, true conformal coverage for all channel surfaces, and simple deposition for cost-effective manufacturing. Future studies will involve the fabrication of ultrathin silicon dioxide layers in field-effect fluid manifolds and the exploration for the use of a hybrid plastic/silicon platform for integrating fluidic networks with functional silicon elements while providing compatibility for mass production at a reduced cost.

CHAPTER THREE

DNA Mutation Detection In A Polymer Microfluidic Network Using Temperature Gradient Gel Electrophoresis

Submitted for publication and reproduced with permission from Analytical Chemistry. Authors: Jesse S. Buch; Christopher Kimball; Frederick Rosenberger; W. Edward Highsmith, Jr.; Don L. DeVoe; Cheng S. Lee.

INTRODUCTION

The nearly completed human genome sequence produced by the Human Genome Project makes available a reference against which all other sequencing data can be compared [7]. As a result, the search for the role performed by specific genes and gene variants in disease has been greatly accelerated, with cancer and genetic disorders serving as the primary targets [3]. At the forefront of this endeavor is the identification of specific nucleotide variations known as single-nucleotide polymorphisms (SNPs). SNPs have attracted the bulk of the attention because they are the most widely distributed form of genetic variation in the human genome and therefore offer the highest resolution markers for tracking disease genes and

population history. These types of single base substitutions, insertions, and deletions in the genome occur at a frequency of greater than 1% in the human population. According to a recent estimate, there are 2.1 million SNPs in the human genome occurring at a density of approximately 1 per 1.25kb of sequence [7].

Continuing progress toward the identification of new genes, the detection of sequence variations in these genes, and the relationship between disease states and these gene variants has garnered high priority. As a result, increasing demand has arisen for the development of technologies that offer greater accuracy, superior cost-effectiveness, and higher throughput than what is currently available. Although, nucleotide sequencing remains the preferred method for detecting and identifying specific nucleotide variations, the rather low frequency of mutations present in the genome renders sequencing a fairly inefficient approach to the large-scale investigation of genomic sequence heterogeneity. Furthermore, the high cost of screening samples for mutations by nucleotide sequencing and the difficulty in detecting heterozygous mutants remain issues.

The most prevalent of the slab gel-based traditional SNP detection techniques include heteroduplex analysis (HA) [63,64], single-strand conformation polymorphism (SSCP) [8,64], and denaturing gradient gel electrophoresis (DGGE) [13]. HA and SSCP have both been successfully implemented in capillary [65,66] and microchip formats [38,39] resulting in increased automaton, efficiency, and speed. Of the three traditional methods however, DGGE has shown the most promise as it can handle longer DNA fragments, is less time consuming, and its

mutation detection sensitivity can theoretically reach 100%. Implementation of DGGE in the capillary format was initially reported by Gelfi and coworkers [67]. A secondary polymer concentration gradient, in addition to the usual denaturant gradient, was employed for refocusing sample bands. Still, the irreproducibility inherent in attaining *in situ* preparation of competent chemical denaturant gradient gel matrices along with the additional secondary polymer concentration gradient required for adequate sensitivity renders implementation difficult.

Temperature gradient gel electrophoresis (TGGE) is analogous to DGGE and has been successfully demonstrated in slab gel [68] and capillary [69-73] formats. Gelfi et al. pioneered generated a temporal thermal gradient in the capillary via joule heating [69]. The joule heating and subsequent temperature in the capillary were manipulated by ramping the separation voltage with time. The inability to control the separation voltage and temperature independently has led to the pursuit of alternative temperature control strategies for TGGE in capillary. Schell and coworkers [70] modified the cooling jacket of a commercial capillary electrophoresis system to allow for the generation of a controlled temperature ramp over time. Gao and Yeung [71] successfully extended this use of an externally generated temporal thermal gradient to a high throughput TGGE system consisting of an array of 96 capillaries. Zhu et al. [73] later demonstrated TGCGE with a spatially generated thermal gradient as well.

In this work, plastic microfluidic systems employing TGGE are developed to perform rapid and cost-effective screening for DNA sequence variation. Bulk heater

assemblies are utilized to externally induce both spatial and temporal thermal gradients in the microchannels, thus enabling single and parallel TGGE separations. Reduced size and power requirements in microfluidics not only lead to improved portability and the effective simplification of equipment requirements, but also establish the foundation for on-chip heater/sensor integration. A comprehensive polycarbonate (PC)-based microfluidic device, containing an integrated microheater and sensor array for generating an internal spatial temperature gradient along the length of the microchannel, illustrates the potential of achieving high throughput and sensitive DNA mutation detection in miniaturized systems.

EXPERIMENTAL SECTION

Materials and Reagents. Boric acid, KlenTaq® DV Ready Mix, and poly(vinylpyrrolidone) (PVP, MW 360,000) were obtained from Sigma (St. Louis, MO). Ethylene(diaminetetraacetic acid) (EDTA) and Tris(hydroxymethyl)aminomethane (Tris) were acquired from Bio-Rad (Hercules, CA). YOYO®-1 fluorescent intercalating dye (excitation: 491 nm; emission: 509 nm) and PCR primers were purchased from Molecular Probes (Eugene, OR) and Integrated DNA Technologies (Coralville, IA), respectively. All aqueous solutions were prepared using water purified by a Nanopure II system (Dubuque, IA) and further filtered with a 0.22 μm membrane (Costar, Cambridge, MA).

Device Fabrication. A standard lithographically patterned silicon master template containing a positive representation of the desired channel network was

used to fabricate the plastic microfluidic devices from blank PC substrates *via* thermal embossing. Briefly, each blank PC disk, 9.0 cm in diameter and cut from 1.5 mm thick PC sheet (Sheffield Plastic, Sheffield, MA) was aligned over the silicon template and the subsequent assembly was sandwiched between two glass plates. A hydraulic press with heated platens was then used to emboss the PC substrate with an applied force of 300 psi at 160 °C for 5 min. A separate PC substrate, complete with machined channel access holes, was aligned with the embossed substrate to serve as a cover piece. The assembly was sandwiched between two glass plates and the previously embossed open channels are sealed by thermally annealing the substrates under 900 psi at 140 °C for 10 min. Finally, fluid reservoirs machined from 1.3 cm-thick PC sheet were fixed to the annealed substrates with epoxy to complete the device. Each fabricated device contained ten distinct microchannels (Fig. 3.1) with the dimensions of 6.0 cm in length, 60 μm in width, and 30 μm in depth.

Temperature Control Schemes. Two different approaches, involving the use of bulk heaters and an integrated microheater, were employed for the generation of both temporal and spatial temperature gradients along the microchannels for

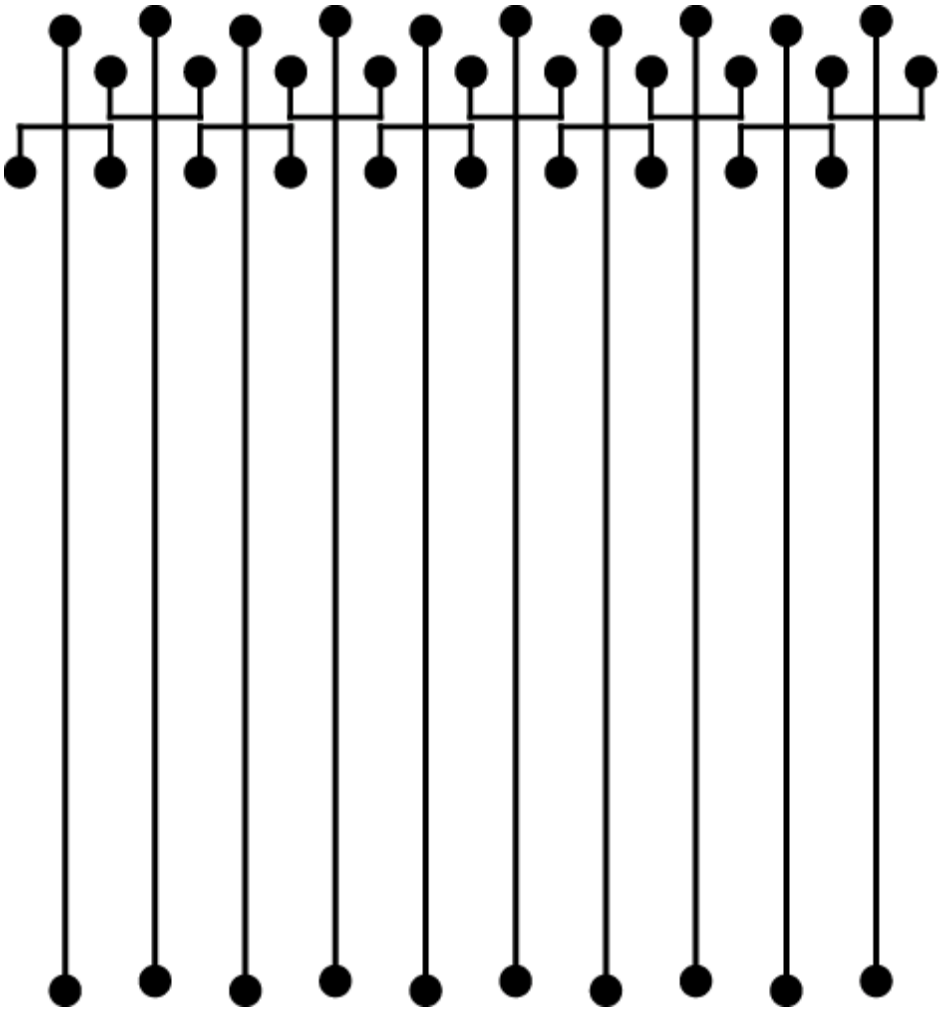

Figure 3.1 Schematic of 10-channel microfluidic device.

performing on-chip TGGE separations. An aluminum heating plate with dimensions of 5.0 cm x 5.0 cm x 0.3 cm was utilized to establish an externally generated temporal temperature gradient. A 10 W silicone rubber heater from Watlow (St. Louis, MO) was mounted on the aluminum plate along with a type-J thermocouple. The heating plate was positioned on the device so that it covered the first 5.0 cm of

the separation channel. Even contact between the top surface of the microfluidic device and heater was achieved by mechanically fixing the heater assembly to the microfluidic device. A Watlow Series 96 single-loop auto-tuning controller was used to ramp the temperature at the desired range and rate during the separations.

A bulk heater platform, similar to the one reported by Mao and coworkers [74], was employed for the separations involving an externally generated spatial temperature gradient. Briefly, a custom aluminum heating plate with dimensions of 12.7 cm x 7.6 cm x 1.3 cm was constructed. The high-temperature end of heating plate was controlled by a 300 W cartridge heater from Omega Engineering (Stanford, CT). The cartridge heater was inserted into one hole at the high-temperature end and was monitored by a Watlow Series 96 single-loop auto-tuning controller with a type-J thermocouple mounted onto the heating plate directly above the cartridge heater. The low-temperature end of the heating plate was manipulated by circulating water through copper tubing that was inserted into the second hole. The water flow rate and temperature were regulated by a water circulator with heating and cooling capabilities from Fisher Scientific (Pittsburgh, PA). The bottom and sides of the heating plate were insulated by a custom plastic housing constructed from black copolyester. Transfer of the induced linear spatial temperature gradient from the surface of the heating plate into the microfluidic separation channels was facilitated by clamping the microfluidic device to the exposed surface of the heating plate with the channel oriented in parallel to the applied thermal gradient.

A comprehensive microfluidic device, containing an integrated microheater and temperature sensor array (Fig. 3.2), was fabricated for the internal generation of a spatial temperature gradient for performing microchip TGGE. Briefly, a thin layer of titanium with a thickness of 20-100 nm was evaporated onto a blank PC substrate. A microfabricated heater and sensor array were then lithographically patterned in the thin titanium layer. A 0.5 μm thick gold layer was similarly evaporated onto the titanium and patterned to form low resistance leads and bond pads. A parylene layer with a thickness of 5-10 μm was then deposited atop the integrated elements. Finally, a second PC substrate, containing embossed microchannels, was sealed by a piece of 25 μm thick LDPE/Nylon lamination film prior to being mechanically fixed to the heater substrate to form the integrated device.

DNA Samples and PCR Reactions. Model ds-DNA fragments ranging in size from 136bp to 530bp and containing SNPs were prepared by amplifying DNA Toolbox plasmid templates [65] via PCR. Briefly, 4 plasmid constructs (40-A, 40-C, 40-G, and 40-T) containing 40%-GC content and differing in sequence at one site to account for all possible SNPs were amplified with the required primers to achieve

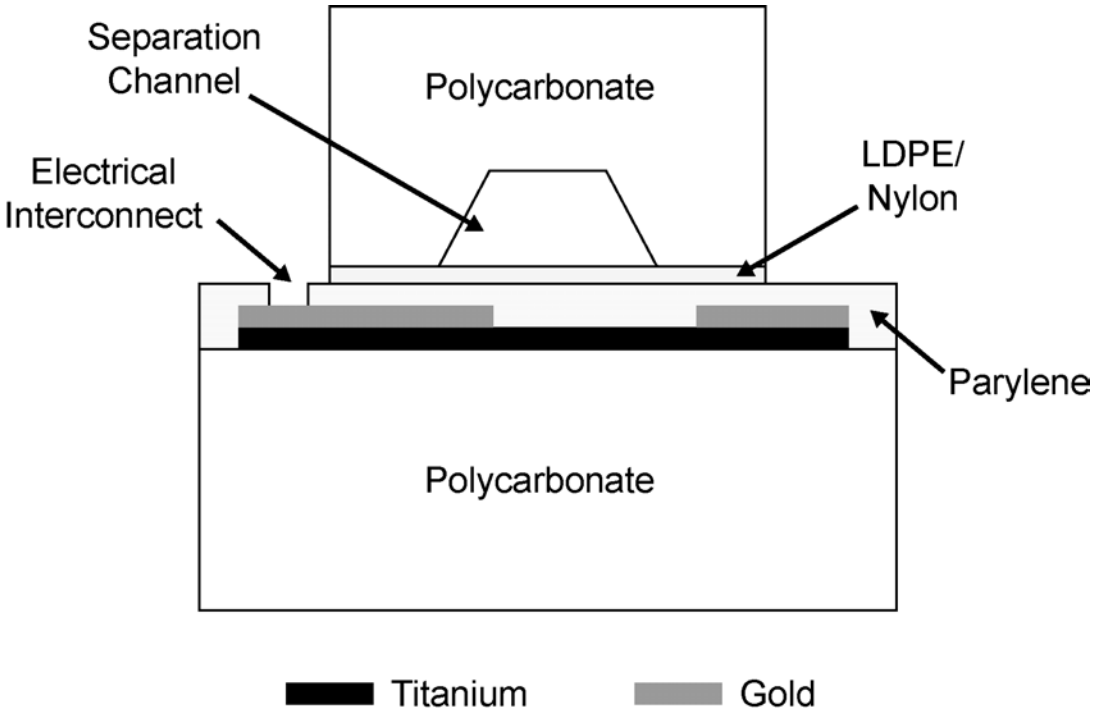

Figure 3.2 Cross-section of the polymer microfluidic device for integrated spatial TGGE analysis. A spatial thermal gradient is established in the separation channel by a tapered microheater and thermal sensor array that are patterned on the bottom polycarbonate substrate of the device.

the desired sequence and size range in fragments. As summarized in Table 3.1, five fragments with the size of 136, 239, 339, 450, and 530bp were named Mut_{100}, Mut_{200}, Mut_{300}, Mut_{400}, and Mut_{500}, respectively. Their melt maps are shown in Figure 3.3 for both the wild type homoduplexes and the mismatched mutant heteroduplexes.

Table 3.1. Characteristics of the DNA Samples

sample name	length (bp)	mutation type	mutation position	primer sequence (5' → 3')
Mut_{100}	136	A to G	89	For =*TCATTCTCGTTTTCTGAACTG Rev = ATGTTTAGACTGGATAGCGT
Mut_{200}	239	C to T	89	For =*TCATTCTCGTTTTCTGAACTG Rev = TAAGAGCAACACTATCATAA
Mut_{300}	339	A to C	110	For = GCAATCCGCTTTGCTTCTGA Rev =*AATGCAGATACATAACGCCA
Mut_{400}	450	C to G	110	For = GCAATCCGCTTTGCTTCTGA Rev =*AGTCAGGACGTTGGGAAGAA
Mut_{500}	530	G to T	301	For=TTGAGCTACAGCATTATATTCA Rev =*AATGCAGATACATAACGCCA

* - primer has a 40bp GC-clamp attached at the 5'-end. Sequence of GC-clamp is as follows: 5' CGCCCGCCGCGCCCCGCGCCCGTCCCGCCGCCCCCGCCCG 3'

One primer in each set was synthesized with a 40bp GC-rich region at the 5'-end for the purpose of artificially introducing a 40-mer GC-clamp at one end of the amplified fragments. All amplifications consisted of a 50 μl reaction volume that included 2.5 mM $MgCl_2$, 1X PCR buffer, 200 μM dNTPs, 1.0 U Taq polymerase, 10 ng of template DNA, and 40 pmol of each primer. Each reaction was executed for 40 cycles using a PE GeneAmp PCR System 9700 (Applied Biosystems, Foster City, CA). Heteroduplex formation was achieved by performing mixed-template PCR as equimolar volumes of each template were coamplified in a single PCR

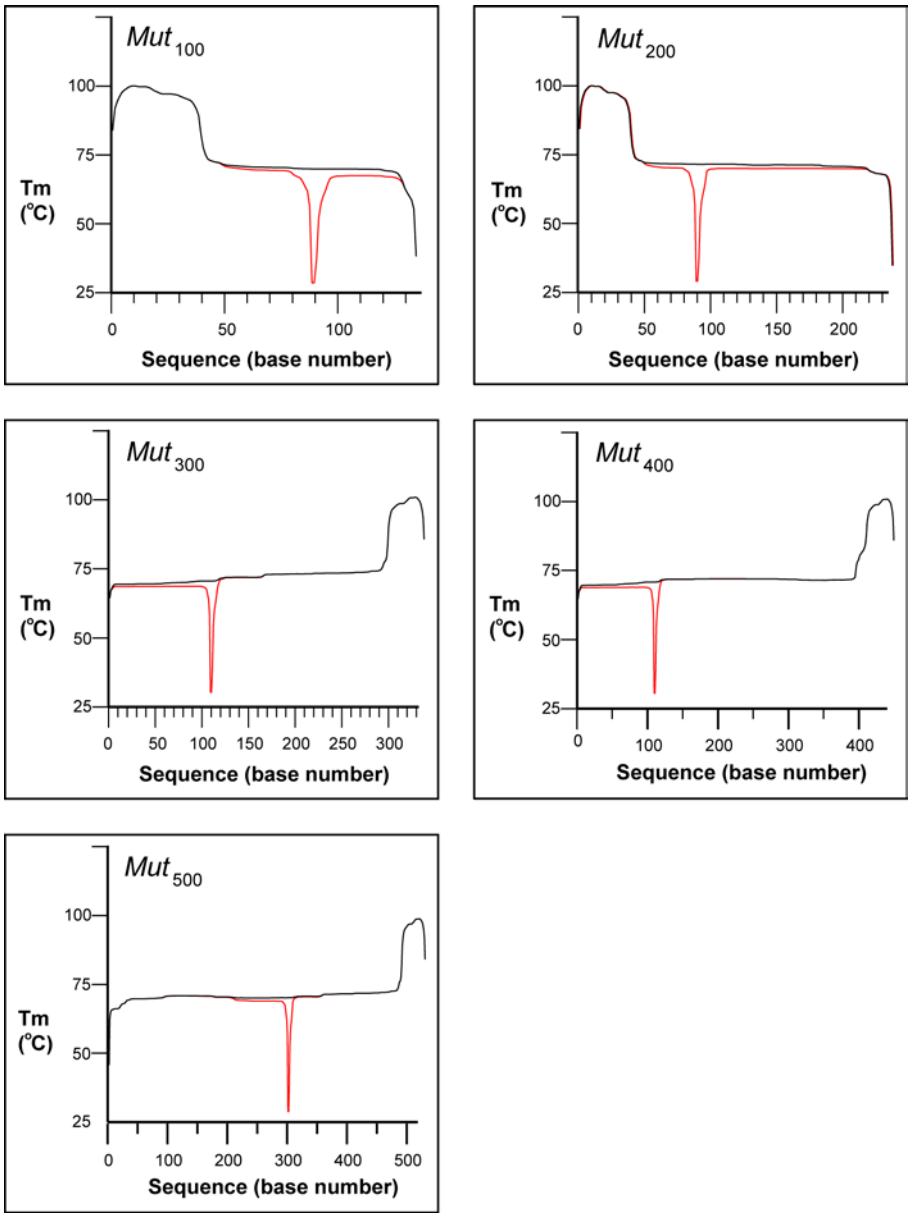

Figure 3.3 Melt maps for the five samples calculated by Poland Analysis software [75]. Traces for each sample representing the wild-type homoduplex (black line) and the mismatched mutant heteroduplex (red line) are superimposed for comparison.

reaction to generate mismatches. The concluding elongation step in the PCR was followed by a final denaturation at 94 °C for 5 min before incubating at 68 °C for 30 min. The amplified DNA was then allowed to cool to room temperature over 1 hr.

TGGE Analysis. The DNA was labeled with YOYO®-1 fluorescent intercalating dye prior to analysis. The microchannels were filled with 4.5% PVP in 1X TBE buffer (89 mM Tris, 89 mM boric acid, 2 mM EDTA) as the polymer matrix. Effective separation lengths were 5.5 and 4.0 cm for the devices using the external heater assemblies and an integrated heater, respectively. Laser-induced fluorescence detection was utilized to monitor the separations with the 488 nm-line of an argon-ion laser. Briefly, a laser-line generator lens (Edmund Industrial Optics, Barrington, NJ) was used to expand the incident laser beam horizontally prior to focusing the beam vertically with a 15-cm focal length cylindrical lens. The orientation of the optically generated laser line was redirected vertically toward the detection window on the PC device where it spanned the 10-channel array on the substrate. The fluorescence was monitored individually in each channel by a 16-bit cooled CCD camera (Andor Technology, South Windsor, CT) employing a 50-mm macro Nikon camera lens to focus the light onto the CCD sensor. A holographic notch filter was located in front of the CCD chip to filter out laser scattering.

RESULTS AND DISCUSSION

TGGE is able to reveal the presence of sequence heterogeneity in a given heteroduplex sample by inducing a thermal denaturing gradient that results in

differences between the average electrophoretic mobilities of DNA molecules that are identical in size, but different in sequence. Given that the melting profile of a DNA molecule is dependent on its sequence, DNA fragments of like size but different sequence denature at different temperatures. When performing electrophoresis under partial melting conditions, individual species display different states of equilibrium between the unmelted DNA fragment and the partially melted form. Because the fraction of time spent by the DNA molecules in the slower, partially melted form varies among specific sequences, less stable fragments exhibit a lower average electrophoretic mobility during the separation than more stable fragments. In this way, the mobility difference induced by the thermal gradient allows TGGE to resolve DNA sequence variants, thus revealing the presence of mutations in a given sample.

The sensitivity of TGGE (and DGGE) has been shown to increase significantly by adding artificial segments known as GC-clamps, 30-50bp stretches of GC-rich fragments, to one or both ends of the DNA fragment targeted for analysis. The GC-clamp can be easily introduced when amplifying the target sequence via the PCR reaction by including it at the 5'-end of one of the PCR primers [14]. In the absence of the GC-clamp, a DNA fragment consisting of a single melting domain denatures completely under the applied temperature gradient, making it impossible to determine any presence or absence of sequence heterogeneity. Additionally, when the DNA fragment of interest consists of multiple melting domains, only mutations in the lowest melting domain are readily

detected. By including a GC-clamp, a single high melting domain is artificially created at one end of the target fragment. When properly positioned, the addition of a GC-clamp can convert the target sequence of a fragment to a single low melting domain ensuring that any mutation present in the target fragment is detectable by TGGE.

To successfully resolve sequence variants in a TGGE analysis, the separation medium must sustain a thermal gradient at a resolution that is finer than the difference in partial melting temperatures among the variants, while performing at a high enough efficiency to maintain the achieved separation through the detection region. Thus, the primary experimental constraint for a proven microfluidic-based TGGE platform is the resolution of the thermal gradient that is applied during the separation. In this study, two separate approaches, involving the use of bulk heaters and an integrated microheater, were pursued toward generating an adequate temporal or spatial thermal gradient for performing TGGE separations in a polymer microfluidic device fabricated from PC.

Externally Generated Temporal Temperature Gradient. To establish a temporal temperature gradient for performing TGGE separations, the channel temperature was regulated by applying heat to the top face of the microfluidic device using a small aluminum heating plate. The accuracy and reproducibility of the temperature control system was confirmed by first calibrating the system. This was accomplished by embedding and monitoring type-J thermocouples in both outer

surfaces of a PC microfluidic device. The thermocouples were positioned so that they were centered in the heated region at identical locations on either side of the device. Assuming the heat transfer to be linear through the device, the temperature in the microchannel was calculated by averaging the temperatures recorded at each outer surface of the device.

Because the thermal conductivity for PC is relatively low (0.2 W/m-K, 14.5% the value for fused silica), a considerable time delay exists between the temperature increase on the surface, at which the heat is applied, and the temperature increase in the microchannel. The temperature in the channel typically required an interval of two min before it reached steady state. Once at steady state, the temperature in the channel was 10 ºC lower than the heated outer (top) surface and it consistently increased at a rate that was 65% of the rate at which heat was applied. As a result, the range and ramp rate of the applied temperature gradient was adjusted to account for the lag time and reduced rate for temperature increase in the channel, in order to achieve the thermal conditions desired for the separations. For example, to achieve a 65.0 ºC to 75.0 ºC temperature ramp in the channel over four min during the separations shown in Figures 3.4 and 3.5, the controller was programmed to heat the top outer surface of the device from 67.3 ºC to 90.4 ºC over 6 min. The sample injections were performed electrokinetically at two min, once the temperature increase in the channel had reached steady state, with the separation carried out over the final four min of the applied temperature ramp. The temporal

temperature gradient was applied over the first 5 of the 5.5-cm long effective separation length.

TGGE Separations were performed in both individual and parallel formats. Figure 3.4 illustrates the reproducibility that was attained for separations of the Mut_{100} sample in the single mode. The reproducibility shown is representative for the entire sample set when analyzed by temporal TGGE in the single mode. Due to the shorter analysis times associated with microchip electrophoresis, the temporal

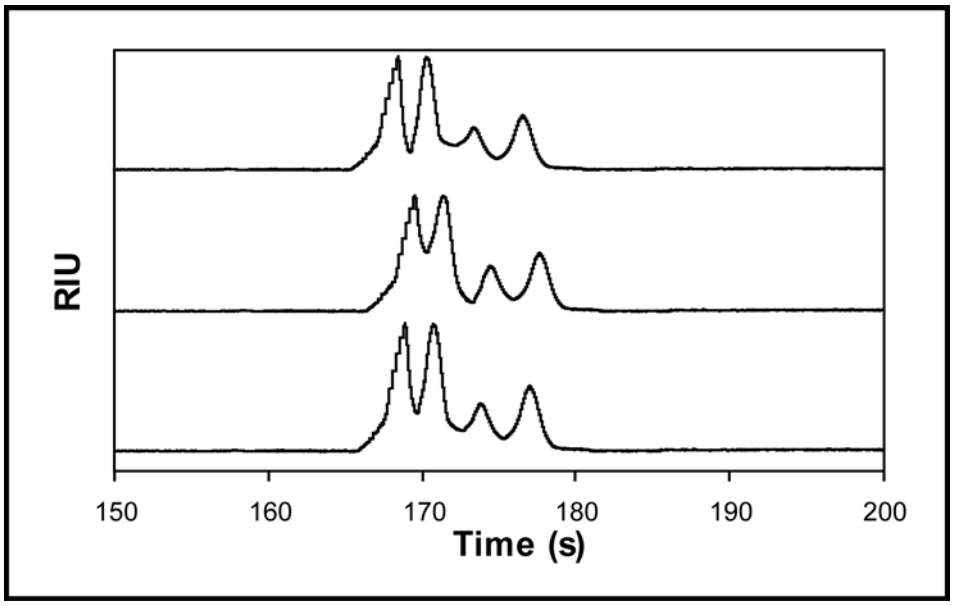

Figure 3.4 Three temporal TGGE electropherograms of *Mut*$_{100}$ sample illustrating the reproducibility of the analysis. Analyses are performed sequentially using 4.5% PVP in 1X TBE under an applied electric field of 150 V/cm. The PVP gel matrix is replaced in the channel prior to each analysis.

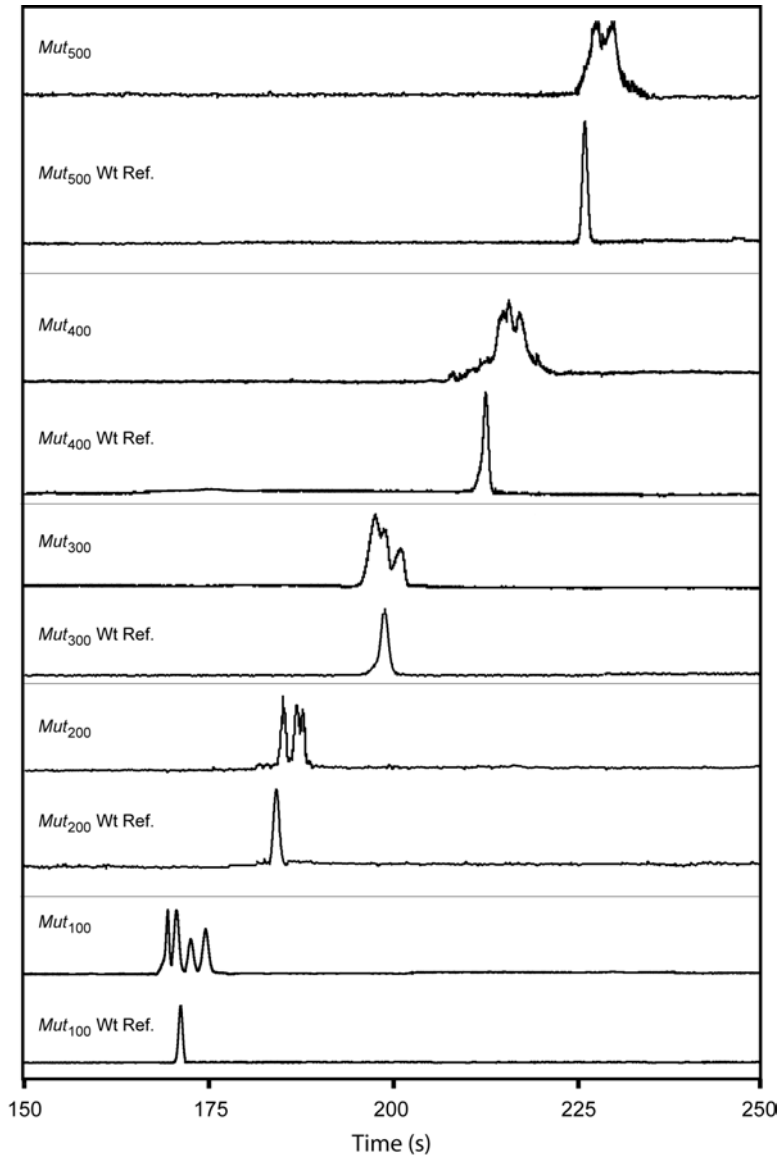

Figure 3.5 Multichannel electropherograms for 10-channel temporal TGGE analysis performed in parallel. Conditions are identical to those described for Figure 3.4.

resolution for the applied temperature ramps is not as high as that for capillary-based temporal TGGE systems [68-71]. However, the much smaller injection plugs associated with microchip electrophoresis require a temporal TGGE system to generate a difference in partial melting between two sequence variants for only a few seconds for those variants to be resolved from one another. This enabled the microfluidics-based temporal TGGE system to attain resolution and separation efficiency that are comparable to capillary TGGE systems, but at a much shorter analysis time.

To demonstrate the applicability of the temporal TGGE platform for performing high throughput mutation detection, all five model mutant samples along with their corresponding reference wild types were analyzed in parallel under one temporal temperature gradient. Although lacking optimal resolution under one temperature gradient, a 10-channel parallel separation positively detected SNPs in all five model mutant samples in less than 4 min. Further enhancement in throughput can be achieved by simply fabricating devices containing a high density of microchannels in the parallel array.

Externally Generated Spatial Temperature Gradient. As discussed earlier, the low thermal conductivity of PC provides a significant impediment when using an external heat source to generate a temporal thermal gradient inside the separation channel. Consequently, the viability of performing TGGE in a PC microfluidic device using an externally generated spatial temperature gradient was explored. The

use of a broad spatial temperature gradient has the potential for reducing the significance of the low thermal conductivity to analysis time by requiring the channel temperature to reach steady state only once prior to the initial run when performing a sequence of separations. This method also ensures that every fragment theoretically experiences the same temperature gradient during a given TGGE analysis regardless of their differences in electrophoretic mobility within the gel matrix. Removing this time dependence further allows for performing separations at higher electric field-strengths and speeds without sacrificing the resolution of the applied temperature gradient.

For this scheme, the microfluidic device is fixed to an aluminum-heating platform containing a thermal gradient along its length. This bulk spatial thermal gradient platform was constructed with a surface that was significantly larger than the PC microfluidic device for the purpose of reducing edge effects. The resulting platform design provided excellent flexibility and linearity for the range and magnitude of the spatial temperature gradients applied. The various gradients employed were calibrated with a specially modified calibration microfluidic device. Briefly, a device was fabricated using the embossing process described previously. However, prior to thermal binding of the embossed PC substrate to the cover piece, small grooves were milled along the center channel and four miniature thermocouples were fixed equidistantly along the length of the channel. The thermocouples embedded in the bonded calibration device were used to acquire a

spatial temperature distribution along the length of the channel when the device was subjected to the externally applied spatial gradient generated by the platform.

Because of the short separation channel length inherent with microfluidic devices, a 10 ºC temperature difference provided insufficient spatial resolution to attain satisfactory separations. As shown in Figure 3.6, positive identification of SNPs with three of the five model mutant samples, Mut_{100}, Mut_{300}, and Mut_{400}, were achieved by applying a temperature gradient of only 5 ^{o}C (from 70 to 75 ^{o}C) over 6-cm long microchannel array. The effective separation length of 5.5 cm was the same as that employed during the temporal thermal gradient experiments. The reduction in migration time was attributed to the application of a higher electric field strength than that employed during the temporal thermal gradient experiments (Figs. 3.4 and 3.5).

The melt maps shown in Fig. 3.3 display the comparative melting profiles of the complimentary wild-type homoduplex and mismatched mutant heteroduplex for each sample group respectively. The melt maps plot T_m as a function of position along the fragment. For the melt maps shown here, T_m is defined as the temperature at which the base number of interest maintains a 50% stacking probability [21]. Melt maps are able to reveal differences in stability within the melting domain for sequence variants and provide some capability for predicting the detection sensitivity for a given TGGE sample set. Based on the melt maps shown in Figure 3.3, the difference in partial melting temperatures between the homoduplex and

heteroduplex species for each of the Mut_{200} and Mut_{500} samples was not wide enough to achieve separation at the same spatial temperature gradient resolution.

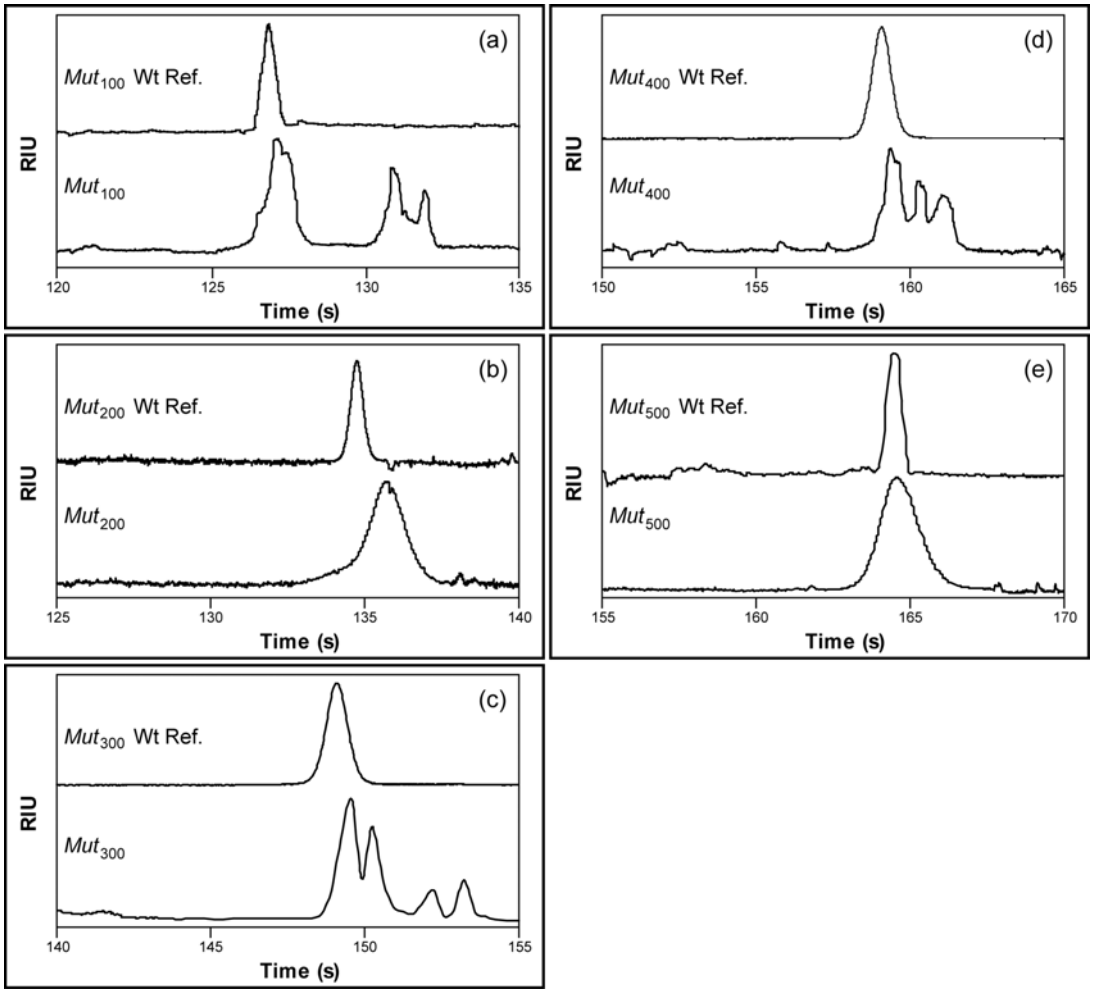

Figure 3.6 Spatial TGGE electropherograms for: (a) Mut_{100}; (b) Mut_{200}; (c) Mut_{300}; (d) Mut_{400}; and (e) Mut_{500} along with their corresponding reference wild type samples. Separations were performed under a spatial thermal gradient of 70-75 ^{o}C at electric field strength of 200 V/cm.

Spatial Temperature Gradient Using Integrated Microheater. One disadvantage to employing off-chip external bulk heater platforms for generation of the thermal gradient is the stipulation that such TGGE systems require off-line calibration and monitoring of the temperature profile imposed in the microchannel. In order to calibrate the thermal gradient applied by an external heating platform, the temperature in the separation channel can be monitored by either introducing a temperature sensitive fluorescent dye [76], or by invasively interrogating the channel environment with a thermocouple probe. Regardless of the approach, it is difficult to replicate the exact experimental conditions of the analysis during calibration. One solution to this problem is to integrate the heaters and sensors directly into to the microfluidic device. By decreasing the proximity of the heaters to the separation channel, the integration of microheaters and sensors on the substrate significantly reduces the power requirement and thermal response times involved in generating an adequate thermal gradient for TGGE separations.

Fabrication of a comprehensive polymer microfluidic TGGE device equipped with an integrated microheater and thermal sensor array was therefore pursued in this study. The spatial temperature gradient was achieved with a tapered heater, and was monitored by an array of 25 resistive temperature detectors (RTD) located next to the heater along the length of the microchannel. The heater was designed such that the power dissipation varied linearly along the length of the heater, establishing a linear spatial thermal gradient in the adjacent separation channel. Each sensor in

the RTD array covered an area of 100 x 300 μm, providing a fine spatial resolution for monitoring the temperature in the channel.

In a preliminary test, the integrated device equipped with a spatial temperature gradient from 70 to 75 ^{o}C over a 4-cm separation length successfully resolved all sequence variants in the Mut_{100} heteroduplex sample (Fig. 3.7). It should be noted that effective separation lengths were 5.5 and 4.0 cm for the devices using the external heater assemblies and an integrated heater, respectively. Compared with the demonstrated external platforms, the increase in the number of sensors from 4 in the

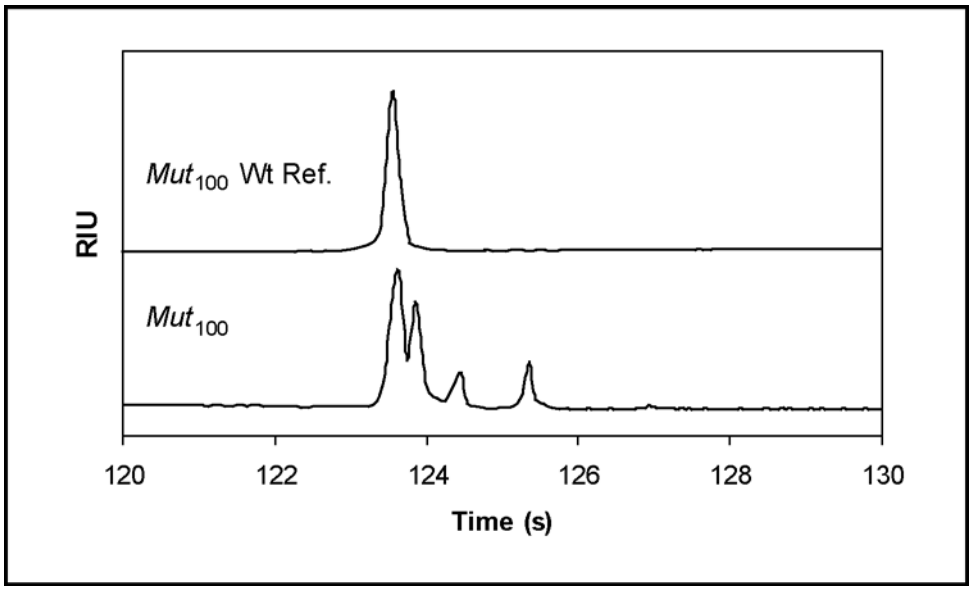

Figure 3.7 Electropherogram for *Mut*$_{100}$ and its corresponding reference wild type sample in a microfluidic device containing an integrated heater and thermal sensor array. The spatial thermal gradient of 70-75 ^{o}C was distributed over a 4-cm long effective separation length at electric field strength of 150 V/cm.

external calibration device to 25 in the integrated approach combined with the reductions in power requirement (50 to 600 times) and thermal response time (50 times) provided more accurate and highly effective control of the temperature gradient, resulting in improved separation efficiency and resolution in a TGGE analysis of the Mut_{100} sample.

CONCLUSION

The demonstrated ability to perform on-chip TGGE analysis of model mutant DNA fragments, each containing a single base substitution at one site, significantly shortens analysis time while achieving resolution comparable to capillary-based systems previously reported in the literature. Two different platforms, involving the use of external heater assemblies and an integrated microheater, are explored for generating temporal and spatial thermal gradients required for performing TGGE separations. The externally generated temporal thermal gradient positively detects sequence variations within all the model heteroduplex samples. Additionally, the temporal TGGE platform is successfully employed in achieving parallel analysis of all mutant DNA fragments, thus further reducing the required analysis time by an order of magnitude in this high throughput format. In contrast, the limited resolution of the externally applied spatial thermal gradient over the short separation length in microfluidic device only allows for the identification of sequence variations in the Mut_{100}, Mut_{300}, and Mut_{400} heteroduplex samples.

The external heater assemblies struggle at quickly generating a thermal gradient due to the low thermal conductivity of polymer substrate and the relatively thick substrate through which the heat is applied to the microchannel. As a result, fabrication of a comprehensive polymer microfluidic TGGE device complete with an integrated microheater and thermal sensor array is pursued. In a preliminary test, the integrated TGGE device rapidly achieves the detection of DNA mutants at better separation resolution and greater energy efficiency than those attained using the external heaters. This comprehensive TGGE microfluidic platform further allows for on-chip control/monitoring of the spatial thermal gradient in the channel during analysis while offering increased potential for portability. Ultimately, the potential of microfluidic technology to transform the conventional and highly sensitive mutation screening method of TGGE into an automated, portable, and high throughput genomic technology is demonstrated.

CHAPTER FOUR

Two-Dimensional Genomic Separations in a Polymer Microfluidic Network

INTRODUCTION

As the scientific community moves forward in the post-genomic era, a primary initiative has been focused on functional genomic studies. At the forefront is the increase in analysis of genetic variation in human populations. This work strives to expand the information and tools at the disposal of healthcare providers with the overall aim of improving disease diagnosis, prognosis, and management. To facilitate the achievement of this goal, the development of enhanced analytical tools for rapid, inexpensive, and accurate detection of DNA sequence heterogeneity had been identified as holding much importance. In addition to the need for more superior analytical technologies, there is also a demand for front-end nucleic acid preparation practices that can be carried out at much higher throughput to minimize any limitations sample preparation steps impose on the overall analysis.

Front-end DNA sample preparation received a tremendous boost from the introduction of the polymerase chain reaction (PCR) in the mid-1980s by Mullis and co-workers [77]. This development revolutionized the field of molecular biology and diagnostics as it provided a means for nucleic acid amplification that is much

more rapid than cloning-based methods. However, when performed in a discrete format (one reaction per reaction volume), PCR can still emerge by far as the rate-determining step in the overall analysis due to the laborious preparation involved. To reduce this, researchers have pursued the implementation of PCR in a more parallel, multiplexed format [20-27]. Under optimized conditions, as many as 10 or more PCR reactions can be carried out in a multiplex fashion within the same reaction volume [20]. Due to the parallel sample processing involved, PCR multiplexing significantly reduces sample preparation time. Furthermore, it provides a procedural means for eliminating much of the variability inherent in the preparation of discreet PCR reactions such as pipetting accuracy and disparity among individual PCR reactions. The ability to perform several reactions in the same volume also provides a significant reduction in reagent consumption, especially with regards to the template DNA.

As a consequence of the establishment of higher throughput biological sample preparation strategies, an even stronger need has arisen for improved analytical technologies capable of resolving highly complex sample mixtures. A popular approach to analyzing complex biological samples such as multiplex PCR products has been to employ two-dimensional gel electrophoresis strategies. A powerful two-dimensional gel electrophoresis methodology was pioneered by Fischer and Lerman [19] and was utilized to fully resolve and detect sequence variations in the entire *E. coli* genome. In this conventional slab-gel approach, DNA fragments can be resolved in two dimensions based on their differences in size

and sequence. DNA fragments in complex mixtures are segregated by size with a standard gel electrophoresis separation in the first separation dimension. Size resolved fragments are then interrogated for sequence variation by a sequence-dependent separation in the second dimension using denaturing gradient gel electrophoresis (DGGE). Apart from nucleotide sequencing, denaturing gradient gel electrophoresis is the only method which provides virtually 100% theoretical sensitivity for mutation detection. In this approach, the application of 2-D DNA gel electrophoresis significantly increases the number of target fragments that can be analyzed simultaneously on the basis of two independent criteria, size and melting temperature (determined by sequence).

By combining extensive PCR multiplexing with 2-D DGGE, Vijg and coworkers have largely enhanced the throughput of 2-D DGGE through the incorporation of a highly parallel sample preparation approach [21,22]. Named two-dimensional gene scanning (TDGS) by its originators, this scheme has been directed toward performing parallel analyses of mutational variants in multiple genes. Accordingly, the exceptional resolving capability of TDGS in the slab gel format has been demonstrated for several large, intensely studied human disease genes, including BRCA1 [22], CFTR [23], RB1 [24], MLH1 [25,26], and TP53 [27].

Although front-end overtures have been made for improving overall throughput of the analysis through the incorporation of multiplex PCR, the fundamental limitations imposed by traditional slab-gel platforms on TDGS prevent the technology from achieving desirable throughput in the analysis step. Despite the

selectivity and sensitivity provided by traditional TDGS, this technique as carried out today consists of a series of manually intensive, time-consuming tasks, which are susceptible to irreproducibility and inferior quantitative accuracy. As a result, higher throughput platforms amenable to multidimensional separation processes have become extremely desirable.

One promising alternative lies in the growing field of microfluidics. Microfluidic analysis platforms are not subject to the fundamental limitations of slab-gel platforms due to their potential for increased miniaturization, automation, resolving power, and speed of analysis. Likewise, the capability of integrating intricate separation networks within a miniaturized platform allows microfluidic technology to readily support the analysis of complex biological samples in a multidimensional, high throughput format.

In the work reported here, a complex single-layer microfluidic network is fabricated in a rigid polycarbonate (PC) substrate for the purpose of performing parallel two-dimensional genetic mutation analyses. In the analysis, standard gel electrophoresis is utilized in the single first dimension channel to provide a size-based separation for model multiplex PCR products of variable size. Following the electrokinetic transfer of the size-resolved PCR products from the first dimension channel into discreet second dimension channels, temperature gradient gel electrophoresis (TGGE) is employed for performing parallel mutational analyses in the second dimension channels. TGGE, analogous to denaturing gradient gel electrophoresis, is performed while externally generating a temporal temperature

gradient through the microfluidic network to provide its sequence-based separation. The thermal gradient provides for the resolution of DNA fragments of similar size, but of different sequence, thus revealing the presence of mutations in a given sample.

To optimize the parallel 2D separation process, extensive finite element modeling (FEM) was performed. The FEM software was utilized to determine the optimal geometries of the microfluidic network for the purpose of minimizing non-uniformities in the electric field and analyte band dispersion caused by the presence of interconnected channels in the microfluidic network. Furthermore, an alternative sample stacking strategy was investigated for increasing the efficiency and resolving power of the overall system for performing genetic mutation analyses.

EXPERIMENTAL SECTION

Materials and Reagents. Boric acid, KlenTaq® DV Ready Mix, Tris(hydroxymethyl)aminomethane hydrochloride (Tris-HCl), fluorescein sodium salt (excitation: 490 nm; emission: 514 nm), and poly(vinylpyrrolidone) (PVP, MW 360,000) were obtained from Sigma (St. Louis, MO). Ethylene(diaminetetraacetic acid) (EDTA) and Tris were acquired from Bio-Rad (Hercules, CA). YOYO®-1 fluorescent intercalating dye (excitation: 491 nm; emission: 509 nm) and PCR primers were purchased from Molecular Probes (Eugene, OR) and Integrated DNA Technologies (Coralville, IA), respectively. All aqueous solutions were prepared using water purified by a Nanopure II system (Dubuque, IA) and further filtered with a 0.22 μm membrane (Costar, Cambridge, MA).

DNA Samples and PCR Reactions. Three model ds-DNA fragments of varying size (136bp, 239bp, and 450bp) and containing SNPs were prepared by amplifying DNA Toolbox plasmid templates [65] via PCR. Briefly, 4 plasmids containing 40%-GC content and differing in sequence at one site were amplified with the required primers to achieve the desired sequence and size range in fragments. As summarized in Table 1 of chapter 3, the three fragments, 136, 239, and 450bp in size, are referred to as Mut_{100}, Mut_{200}, and Mut_{400} respectively. Their melt maps are also shown in Fig. 3 of chapter 3 for both the wild type homoduplexes and the mismatched mutant heteroduplexes.

One primer in each set was synthesized with a 40bp GC-rich region at the 5'-end for the purpose of artificially introducing a 40-mer GC-clamp at one end of the amplified fragments. All amplifications consisted of a 50 μl reaction volume that included 2.5 mM $MgCl_2$, 1X PCR buffer, 200 μM dNTPs, 1.0 U Taq polymerase, 40 ng of template DNA, and 40 pmol of each primer. Each reaction was executed individually for 40 cycles using a PE GeneAmp PCR System 9700 (Applied Biosystems, Foster City, CA). Heteroduplex formation was achieved by performing mixed-template PCR as equimolar volumes of each template were coamplified in a single PCR reaction to generate mismatches. The concluding elongation step in the PCR was followed by a final denaturation at 94 °C for 5 min before incubating at 68 °C for 30 min. The amplified DNA was then allowed to slowly cool to room temperature over 1 hr. Following amplification and heteroduplex formation, the

PCR products from each reaction were desalted using centrifugal membrane filtration to decrease the conductivity of the sample matrix. Finally, the individual PCR products were pooled to simulate an aliquot from a multiplex PCR reaction.

Device Fabrication. A standard lithographically patterned silicon master template containing a positive representation of the desired channel network was used to fabricate the plastic microfluidic devices from blank PC substrates via thermal embossing. Briefly, each blank PC disk, 9.0 cm in diameter and cut from 1.5 mm thick PC sheet (Sheffield Plastic, Sheffield, MA) was aligned over the silicon template and the subsequent assembly was sandwiched between two glass plates. A hydraulic press with heated platens was then used to emboss the PC substrate with an applied force of 300 psi at 160 °C for 5 min. A separate PC substrate, complete with machined channel access holes, was aligned with the embossed substrate to serve as a cover piece. The assembly was sandwiched between two glass plates and the previously embossed open channels are sealed by thermally annealing the substrates under 900 psi at 140 °C for 10 min. Finally, fluid reservoirs machined from 1.3 cm-thick PC sheet were fixed to the annealed substrates with epoxy to complete the device.

Temporal Temperature Control. As described in chapter 3, an aluminum heating plate with dimensions of 5.0 cm x 5.0 cm x 0.3 cm was utilized to establish an externally generated temporal temperature gradient. A 10 W silicone rubber

heater from Watlow (St. Louis, MO) was mounted on the aluminum plate along with a type-J thermocouple. The heating plate was positioned on the device so that it covered from 1.0 cm to 6.0 cm along the length of the second dimension channels moving away from the first dimension channel. Even contact between the top surface of the microfluidic device and heater was achieved by mechanically fixing the heater assembly to the microfluidic device. A Watlow Series 96 single-loop auto-tuning controller was used to ramp the temperature at the desired range and rate during the separations.

Finite Element Modeling**.** The software used to model the electric field profile at the interface between the channels of the first and second separation dimensions was ANSYS 6.1. The software employed to model the dispersion of analyte bands during the first dimension separation and transfer steps was FemLab 2.3. All constants used to define the boundary conditions for the simulations such as conductivity of the electrophoresis medium and electrophoretic mobility of the analytes were determined empirically. The constant used for the coefficient of diffusion was taken from the literature [81].

2D Microfluidic Mutation Analysis. The DNA was labeled with YOYO®-1 fluorescent intercalating dye prior to analysis. The microchannels were filled with 4.5% PVP in 1X TBE buffer (89 mM Tris, 89 mM boric acid, 2 mM EDTA) as the polymer matrix. Effective separation lengths were 6.5 cm for the first dimension

separation and 6.5 cm for the parallel second dimension separations. Briefly, a sample plug was injected into the first dimension separation channel using the pinched-valve injection method [82]. Upon resolution of the sample components by size, the voltage sources controlling the first dimension electrophoretic separation were shut off, halting the electrokinetic migration of the analyte bands. Immediately, the voltage sources controlling the second dimension separation were initiated, and the bands were transferred into discreet second dimension channels where parallel TGGE analyses were performed on each resolved analyte species as the temperature in the channels was ramped over the desired range. A custom-designed laser-induced fluorescence detection system, as described in chapter 3, was utilized to monitor the parallel separations simultaneously. The effective length of the parallel separations was 6.5 cm. Data was recorded at a frequency of 10 Hz.

pH-Mediated Sample Stacking Following Transfer to Second Dimension. Size-resolved analyte PCR bands were stacked following transfer to the second dimension by utilizing the base stacking on-column sample concentration approach introduced by Swerdlow and coworkers [83]. For this process, the sieving matrix for the two-dimensional separation was 4.5% PVP dissolved in 50 mM Tris-HCl buffer. Following the first dimension separation, the transfer process is performed for 10 seconds before being halted. The grounding voltages helping to drive electrophoresis in the second dimension are removed from the buffer reservoirs and applied to reservoirs containing 0.1 N NaOH. NaOH is then injected into each

channel of the second dimension array for a total of 10 seconds before the electric field is turned off and the voltages are reapplied to the buffer reservoirs. The parallel TGGE analyses are then carried out in the same manner as described above.

RESULTS AND DISCUSSION

The promise shown by microfluidic platforms for realizing multidimensional separations in a single integrated system has prompted several research groups to explore such strategies. Recently, researchers have confirmed this potential through preliminary demonstrations of multidimensional protein and peptide separations. These attainments further uphold the potential of microfluidic platforms in providing several unique advantages over traditional bench-top instrumentation and methodologies, including rapid and high throughput separations, ultrahigh separation efficiency and resolution, improved reproducibility, ultralow sample consumption, high sensitivity, and fully automated and integrated operation.

For example, Ramsey and co-workers [78] have demonstrated two-dimensional separations of peptide mixtures in a glass microfluidic device using micellar electrokinetic chromatography and zone electrophoresis as the first and second dimensions, respectively. They have also fabricated a spiral shaped channel coated with a C-18 stationary phase for performing reversed-phase chromatographic separations of tryptic digest peptides. By utilizing a cross interface, the eluted peptides from micellar electrokinetic chromatography or reversed-phase chromatography channel are sampled by a rapid zone electrophoresis separation.

Additionally, Kenny and co-workers have recently coupled isoelectric focusing with zone electrophoresis for 2-D separations of model proteins using plastic microfluidics [79]. In both cases, the multidimensional separations were performed in a serial format. The serial coupling of two dynamic separation methods, as in the work by Ramsey et al., suffers from the fundamental limitation that the second dimension separation must be orders of magnitude faster than the first dimension separation in order to sample the entire volume of the first dimension contents at a high enough density. Furthermore serial two-dimensional microfluidic separation strategies lack the ability to simultaneously sample all analyte bands resolved in the first dimension for parallel analysis in the second dimension, thus falling short of providing maximum throughput.

As an early step toward realizing parallel two-dimensional microfluidic separations, Whitesides and co-workers [80] have developed a 2-D capillary electrophoresis system based on a 6-layer PDMS microfluidic system. The system consisted of a single first dimension channel for performing isoelectric focusing. The single first dimension channel is intersected by an array of parallel channels for achieving SDS gel electrophoresis. This 6-layer PDMS microfluidic system, however, requires the alignment, bonding, removal, re-alignment, and re-bonding of various combinations of the six layers to perform a full 2-D protein separation. In addition to being cumbersome and fairly complex to implement, the system may suffer from band broadening due to diffusion during the post-separation assembly process and cross-contamination during these manual procedures.

For the throughput potential of multidimensional microfluidic separations to be realized, the development of more comprehensive, autonomous, and automation-amenable parallel 2D microfluidic systems is essential. To this end, parallel two-dimensional genetic mutation analysis in a complex, single-layer microfluidic network fabricated in a rigid PC substrate is demonstrated in this study.

Parallel 2D Microfluidic Network Design. The channel network design utilized in the microfluidic system reported here is illustrated in Figure 4.1. Briefly, a single first dimension separation channel (connecting reservoirs 3 and 4), 6.5 cm in length, 100 μm wide, and 30 μm in height is intersected 0.5 cm from the inlet end by a cross injection channel (connecting reservoirs 1 and 2), 1.0 cm in length, 40 μm wide, and 30 μm in height. The cross injection channel provides the structural means for performing the pinched-valve injection required to introduce a sample plug into the first dimension for subsequent separation. The top side of the first dimension separation channel is intersected toward the outlet end by an array of eleven orthogonal 2D fluid access channels that connect the 1D separation channel to the 2D inlet reservoirs (reservoirs 5). These channels are 0.5 cm in length, 40 μm wide, and 30 μm in height. The bottom side of the first dimension separation

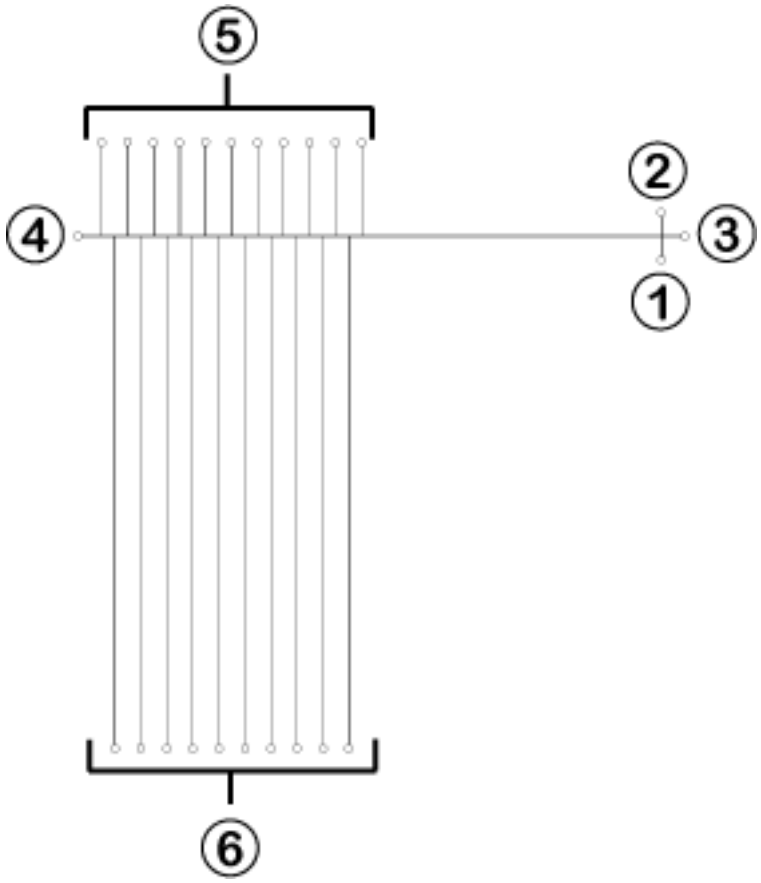

Figure 4.1 Design of two-dimensional microfluidic network. The individual and pooled reservoirs are labeled as follows: 1 – sample reservoir; 2 – waste reservoir; 3 – 1D inlet reservoir; 4 – 1D outlet reservoir; 5 – 2D inlet reservoirs; 6 – 2D outlet reservoirs.

channel is further intersected by an array of ten orthogonal 2D separation channels that connect the 1D separation channel to the 2D outlet reservoirs (reservoirs 6). Each of these channels intersects the first dimension separation channel at the midpoint between the two 2D fluid access channels positioned above on either side. The 2D separation channels are all 7.0 cm in length, 40 μm wide, and 30 μm in height.

The placement of the 2D fluid access channels and the 2D separation channels are staggered with respect to each other to simplify the transfer process. Furthermore, this configuration allows for the entire contents of the first dimension separation channel between the two outermost 2D fluid access channels of the upper array to be transferred into the second dimension in a single process where it can be simultaneously interrogated among ten discreet microchannels by parallel TGGE.

Finite Element Modeling of Network Geometry. To perform a parallel, multidimensional analysis in a microfluidic device, a first dimension separation must be conducted through a channel that is intersected by numerous second dimension channels. The presence of numerous t-junctions within the first dimension separation channel results in discontinuous sidewalls along the length of the first dimension channel. Consequently, the effect these channel junctions have on the separation efficiency of an analyte band as it migrates through them was investigated.

The presence of discontinuous sidewalls in the first dimension separation channel due to the intersecting 2D channels results in a non-uniform electric field distribution along the length of the channel. Similar to a "leaky" electric field, this electric field non-uniformity results when the electric field lines encounter regions of reduced confinement created at the t-junctions along the 1D separation channel by the intersecting 2D channels. At each junction, the uniform density of the

electric field lines is compromised as those nearest to the side channel spread out and follow a parabolic path through the opening to the side channel (Fig. 4.2a).

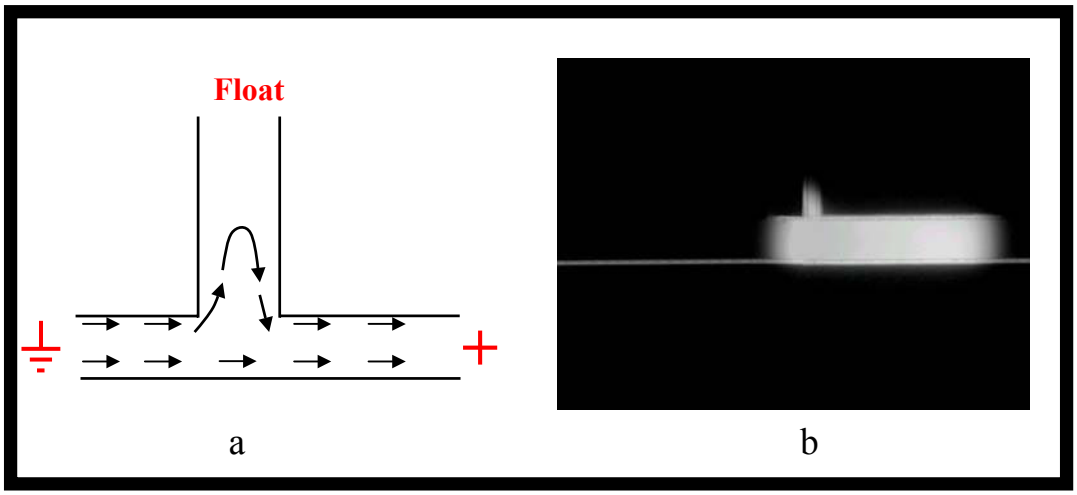

Figure 4.2 a) Cartoon of electric field profile in separation channel at T-junction with a floating, orthogonal channel. b) Image of 10mM fluorescein band illustrates how leakage of the electric field lines into the side channel at a t-junction results in a differential pathlength for the analyte molecules through the junction leading to broadening of the sample band.

Because the separation is driven by the electric field, this electric field non-uniformity causes dispersion of the sample bands in two ways as they migrate through the first dimension separation channel. First, the sample band is dispersed due to the differential electrophoretic velocities experienced among homogenous molecules as they enter a non-uniform electric field region. Secondly, the parabolic path followed by some of the electric field lines through the opening to the side

channel results in differential path lengths for the analyte molecules themselves, thus contributing to the dispersion of the sample bands. This dispersion caused by non-uniformity in the electric field is significant and ultimately results in lower efficiency and resolution for the first dimension size-based separation.

To minimize this sample dispersion phenomenon, finite element modeling using ANSYS 6.1 and FemLab 2.3 software was utilized to look at the effect the ratio of 2D side channel width to 1D separation channel width had on distortion of the electric field at the 2D channel junctions and the resultant broadening of the sample band.

The variation in pathlength experienced by analyte molecules of a given homogeneous sample band is proportional to the depth of leakage by the electric field lines into the 2D side channel at a t-junction. Therefore, minimizing the depth of leakage of the electric field lines into the 2D side channels minimizes the variability in pathlength among the sample molecules. As demonstrated by Figure 4.3, one way to accomplish this is to decrease the width of the side channels with respect to the main separation channel. Furthermore, the ability to minimize the distortion of the electric field across the width of the main separation channel in the t-junction reduces dispersion of a sample band as it migrates through the junction by diminishing the variation in electrophoretic velocities experienced by the homogenous sample molecules. Again, this can also be accomplished by decreasing the width of the side channels with respect to the main separation channel. Contour plots of the electric field profiles for t-junctions of varying width ratios affirm this

relationship in Figure 4.4. Additional finite element modeling and empirical testing to characterize the relationship between actual sample band dispersion and t-junction width ratios (Fig. 4.5). In this work, simulations were performed using FemLab 2.3 to determine predicted band broadening. Parameters and boundary

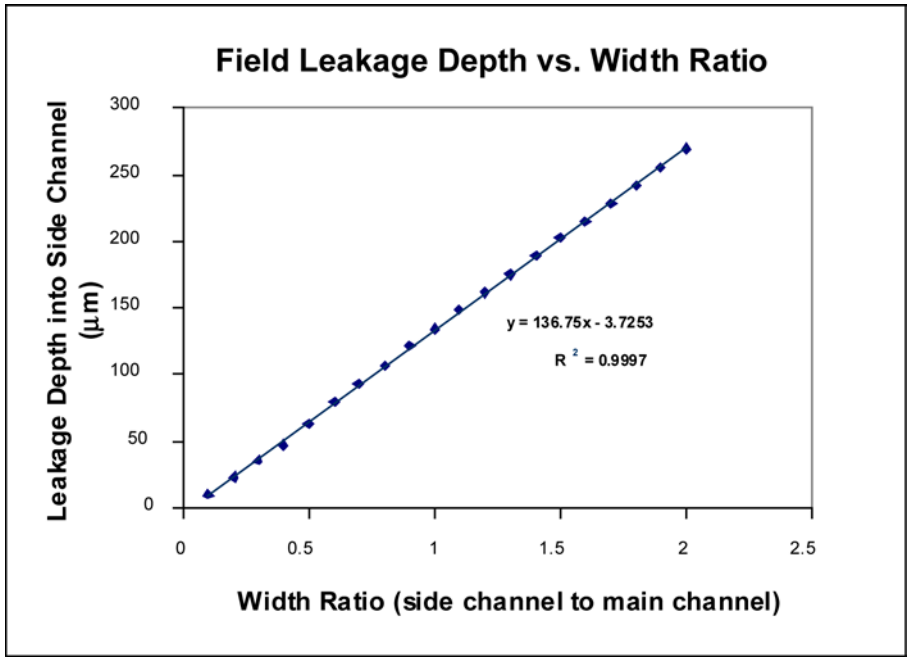

Figure 4.3 Plot of the depth an electric field leaks into the side channel of a t-junction for a given ratio of side channel width to main (separation) channel width. The field leakage depth was determined by measuring the distance into the side channel at which the magnitude of the electric field in the side channel equaled 1% of the electric field in the uniform part of the separation channel.

conditions were established in an attempt to replicate empirical conditions as much as possible. The notable flaw is that the simulations were performed using simplified planar two-dimensional channel geometry with the cross-section of the channel was given a specified width, but no height. In reality, the channels have a three dimensional geometry with a trapezoidal cross-section. This added geometric dimension contributes additional distortion of the electric field in the t-junction that is unaccounted for by the simulations.

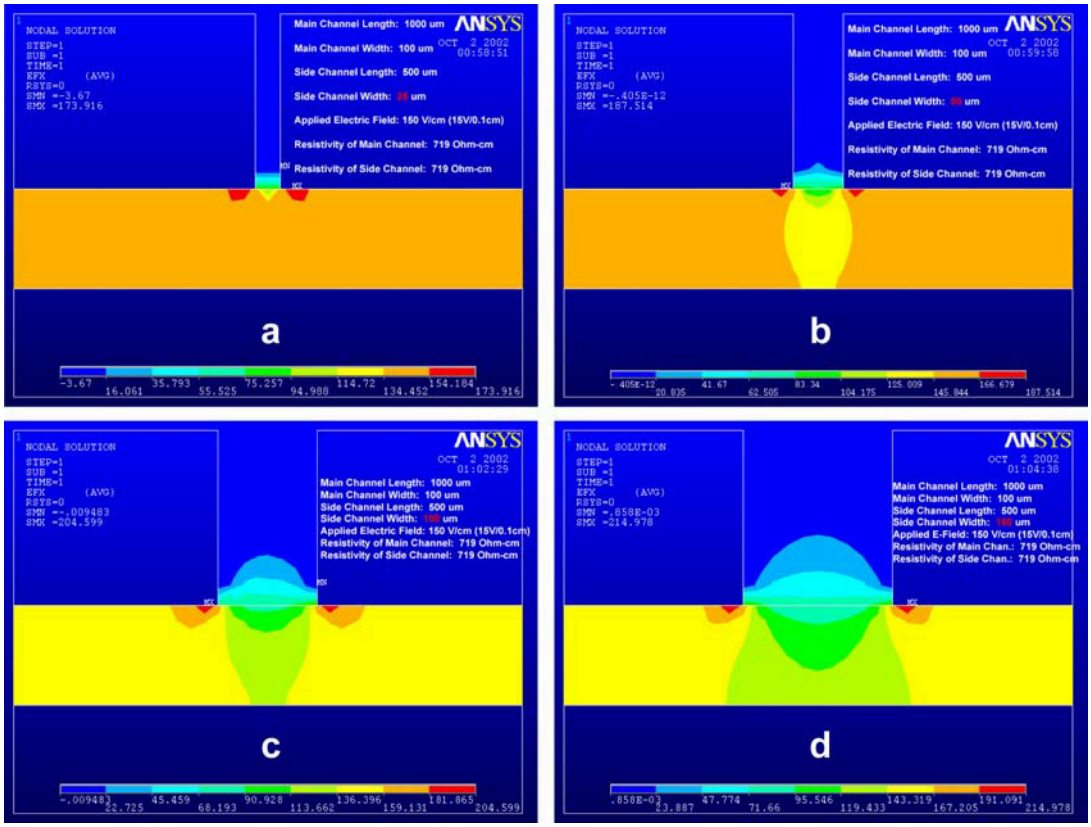

Figure 4.4 Contour plots of the electric field profiles for t-junctions of width ratios: a) 0.1; b) 0.5; c) 1.0; d) 1.5.

The band broadening simulations reconfirmed the relationship that was deduced from the electric field modeling. As is the case for electric field leakage depth and electric field distortion, Figure 4.5 demonstrates that the relative broadening of a sample band as it passes through a t-junction is directly proportional to the ratio of side channel width to separation channel width. Empirical

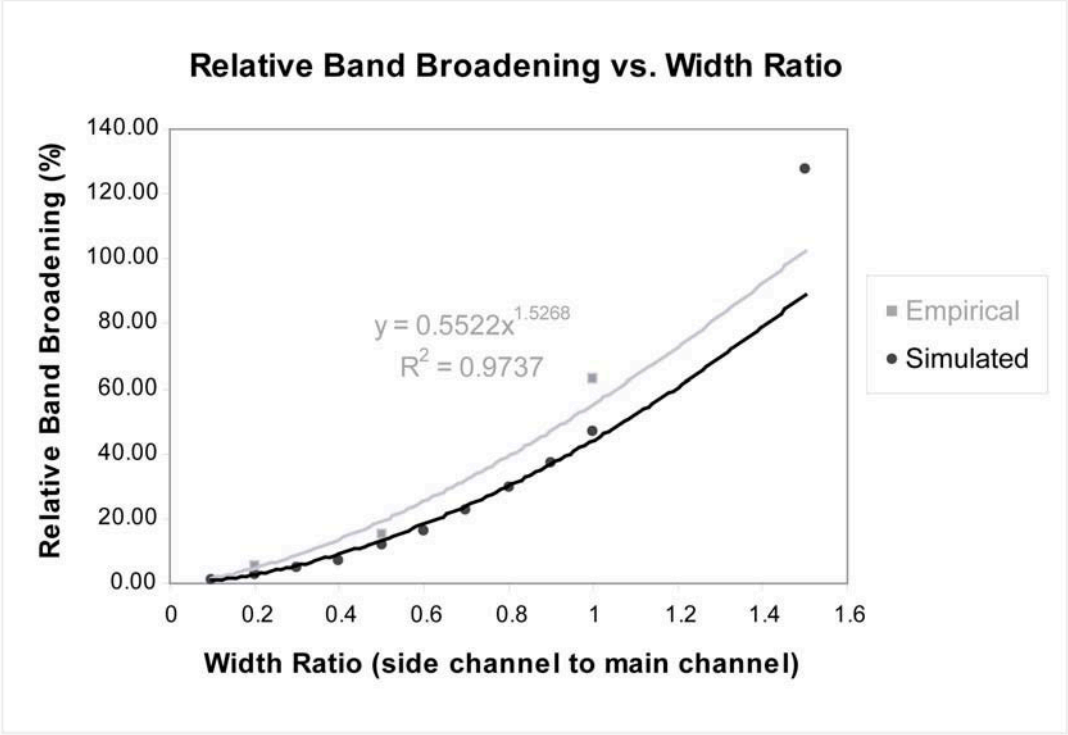

Figure 4.5 Plots of the simulated and empirical sample band dispersion caused by the presence of a t-junction in the separation channel as a function of the ratio of side channel width to separation channel width. Empirical data was only obtained for width ratios of 0.2, 0.5, and 1.0.

measurements, however, exceeded the predicted values considerably. This most likely resulted from the failure of the simulation to account for the three-

dimensional geometry of the channel structure used in the empirical testing. Specifically, for the width ratio used in the 2D microfluidic network demonstrated for genetic mutation analysis in this study (0.4 width ratio), the empirically derived relationship predicts a relative sample band dispersion of 13.63% for each t-junction encountered by the band. Conversely, simulation results predict a sample band dispersion of 7.02% for each t-junction encountered by the band.

Comprehensive Parallel 2D Microfluidic Analysis. A model system consisting of three, sequence variable PCR products 136, 239, and 450bp in size was employed to validate the capability of the demonstrated microfluidic system to perform a parallel 2D genetic mutational analysis. In order to perform a parallel 2D separation in the microfluidic network designed here, the reservoirs used to control the separations must be electrically decoupled from one another. The simplest way to achieve this is to have the terminal ends of every channel in the network disconnected (i.e. no common reservoirs). This allows electrical biases to be selectively applied to, or removed from, reservoirs as needed depending upon the intended operation. The application and removal of voltage sources at selected reservoirs can be accomplished manually by simply placing or removing electrodes by hand. However, this approach is highly undesirable and becomes impractical when the density of channels in the microfluidic network increases. An alternative approach that is highly amenable to automation involves the use of high voltage relays [83]. Relays are inserted in series between the voltage source and the

electrode addressing each reservoir (Fig. 4.6), providing a means for toggling each reservoir as desired between electrically biased and electrically floating states.

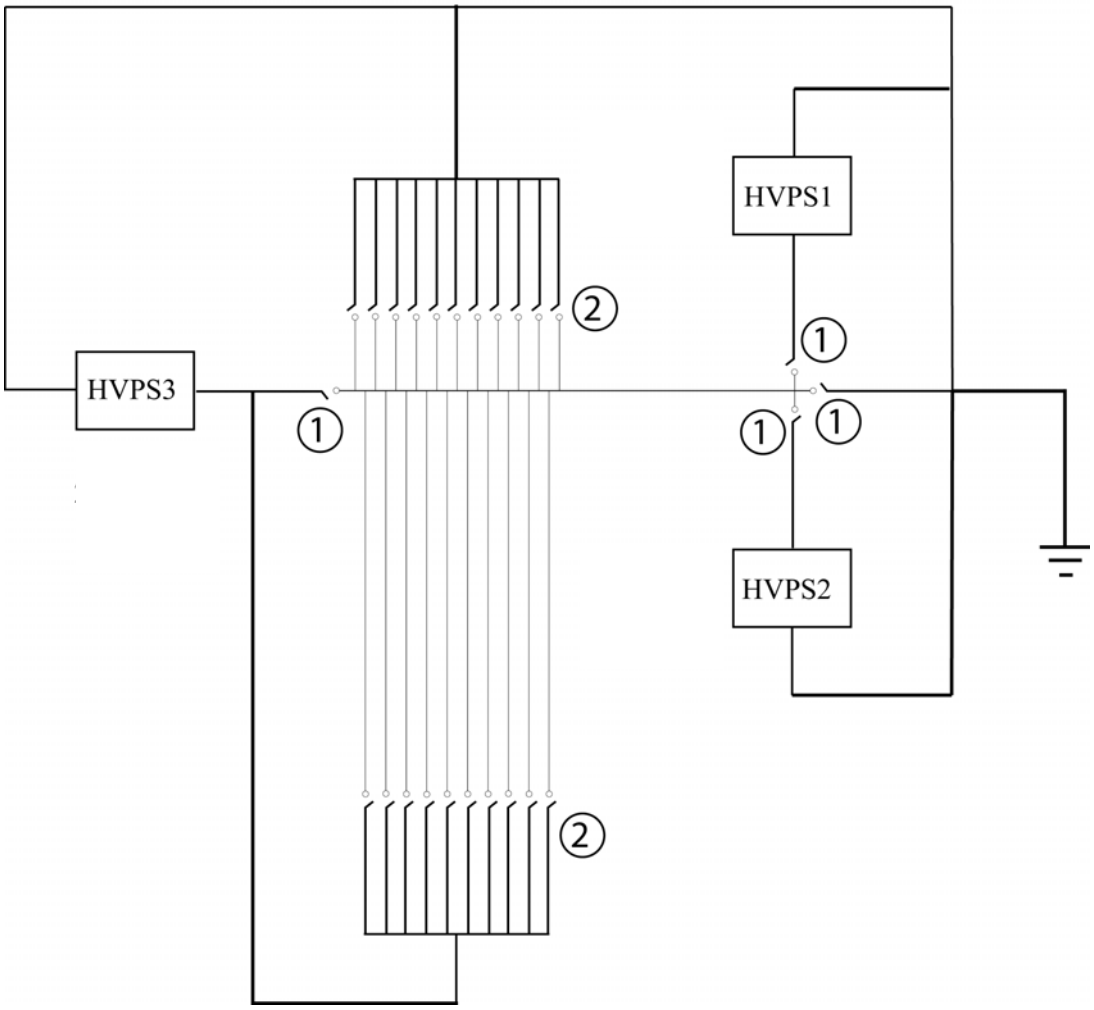

Figure 4.6 2D separation electrical control configuration. Number indicates which 5V power supply controls the high voltage relays. In general, relays for reservoirs involved in the first dimension are closed at the beginning of the 2D separation process and open during the second dimension TGGE separation.

In employing this system to perform a parallel 2D microfluidic genetic mutation analysis, a sample band (~50 μm in width) containing a mixture of three variable-sized PCR products was injected into the first dimension separation channel using a pinched-valve injection technique. The size-based first dimension gel electrophoresis separation was run for 90 seconds allowing for sufficient enough resolution of the PCR products to transfer them into discreet second dimension channels. After 90 seconds, the separation was halted. The reservoirs involved in the first dimension separation (1 through 4 in Fig. 4.1) were then switched so that they were electrically floating with respect to the circuit in the microfluidic network. Next, the reservoirs involved in the second dimension separation (5 and 6 in Fig. 4.1) were then switched so that they could apply an electric potential across the 2D separation channels. In this mode, the transfer and subsequent parallel mutation analysis of all bands is performed simultaneously. Figures 4.7a (homoduplex control) and 4.7b (heteroduplexes) show the results of comprehensive 2D separations for mixtures containing Mut_{100}, Mut_{200}, and Mut_{400}. The mixtures were separated in the first dimension by size for 90 seconds at an electric field strength of 150V/cm. Upon halting the first dimension separation, the size-resolved bands were transferred simultaneously into the second dimension and subsequently separated by sequence using parallel TGGE at 125 V/cm. TGGE was performed with an externally generated temporal thermal gradient by ramping the temperature from 72°C to 75°C over three minutes. An average separation efficiency of ~18,000 theoretical plates was demonstrated for the 2D analysis of the heteroduplex. In the

heteroduplex analysis, the 2D separation successfully revealed all three heteroduplex samples. Each size variant was interrogated for sequence heterogeneity in its own second dimension channel. Total analysis time was under five minutes.

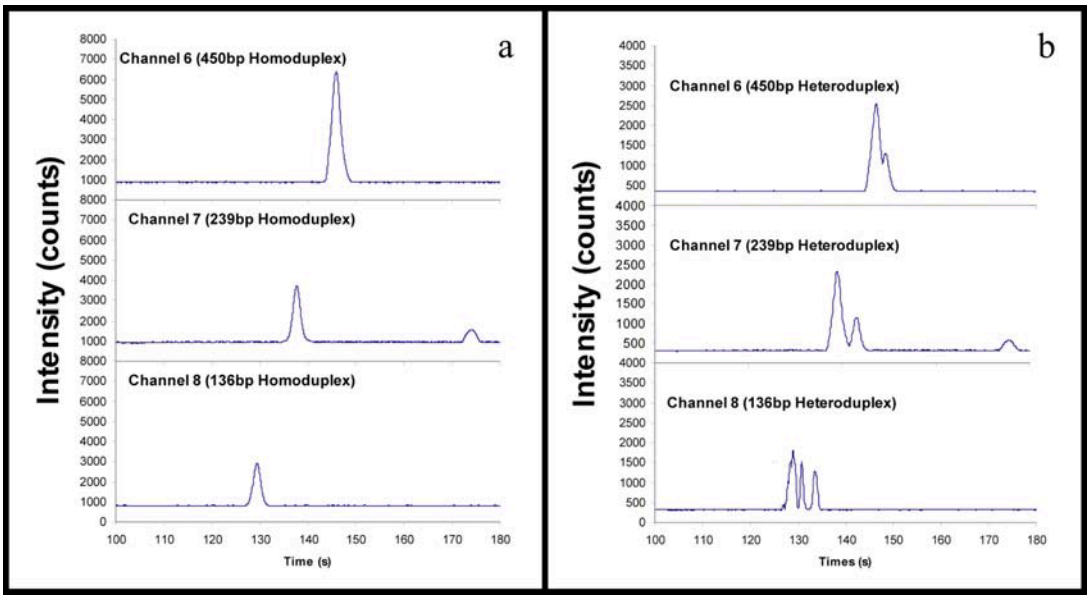

Figure 4.7 Electropherograms for comprehensive 2D DNA separations of a) homoduplex control and b) heteroduplex samples consisting of a mixture of Mut_{100}, Mut_{200}, and Mut_{400} fragments. The time domain along the x-axis of the electropherogram represents the retention time for the second dimension separation only. Data recording was initiated once transfer of bands from first dimension to second dimension commenced. First dimension separation was performed for 90 seconds.

Second Dimension pH-Mediated Base Stacking Approach. An alternative sample stacking strategy was investigated for increasing the efficiency and resolving power of the overall system for performing genetic mutation analyses. This approach utilizes the technique proposed by Swerdlow and coworkers [84] that achieves on-column concentration of DNA fragments by electrokinetic injection of hydroxide ions. Briefly, the separation buffer used is 50mM Tris-HCl in lieu of 1x TBE. As hydroxide ions are injected into the systems, a neutralization reaction occurs between OH^- ions and the cationic buffer component $Tris^+$ as the hydroxide ions migrate through the channels. This results in a dynamic, sweeping zone of lower conductivity that induces an electric field focusing effect upon the DNA bands at the front of this low conductivity zone. The entire process is illustrated in Figure 4.8.

Integrating this pH-mediated base stacking technique into the comprehensive 2D separation system involved modification of the microfluidic network design to accommodate an additional set of reservoirs placed in parallel with group 5 (Fig. 4.1). The modified microfluidic network design is shown in Figure 4.9. Likewise, the separation protocol was adjusted as well.

In performing a comprehensive 2D analysis while integrating this sample stacking method, the first dimension size-based separation was performed exactly as demonstrated previously. A pinched-valve was performed to introduce a sample plug into the first dimension separation channel where the size variants within were subsequently resolved. After 90 seconds, the first dimension separation was halted

and the bands were electrokinetically transferred into second dimension channels for 10 s before the field was turned off. As illustrated in Figure 4.8, the electric potential was removed from the buffer reservoirs and placed in the NaOH reservoirs upon which NaOH was injected into the second dimension separation channels for

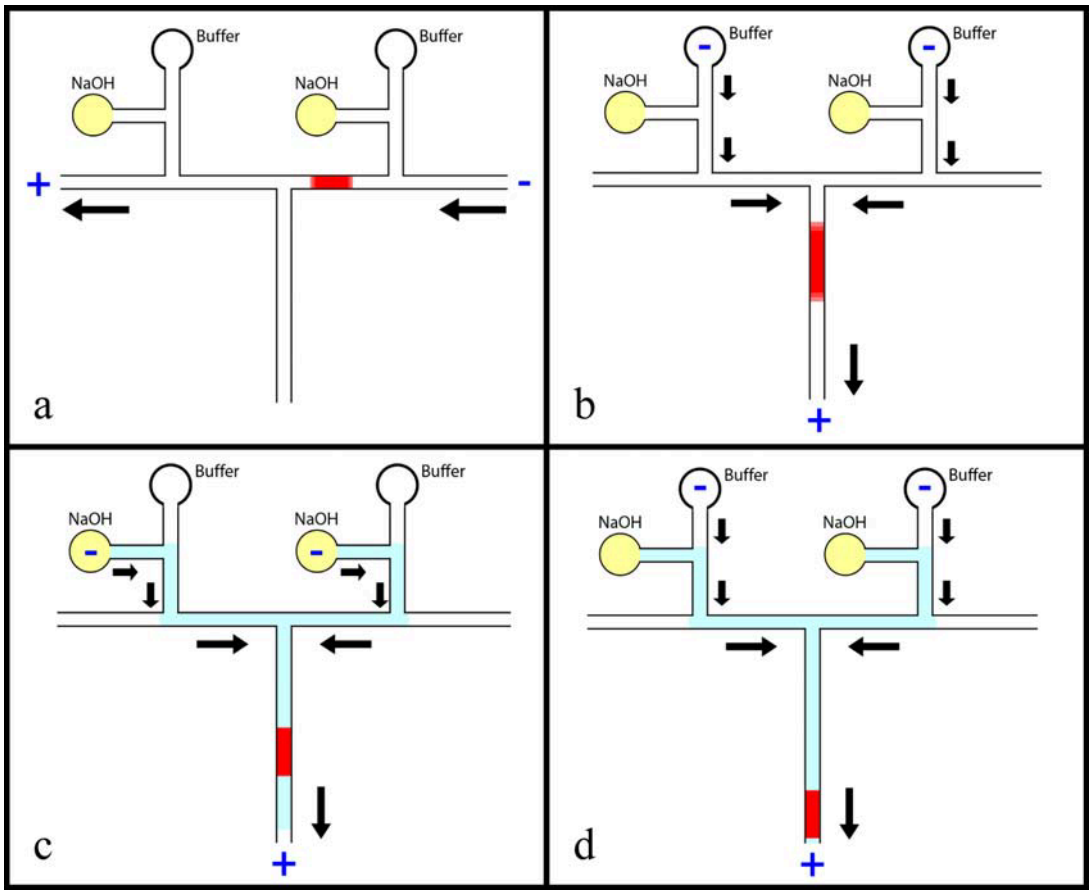

Figure 4.8 Illustration of the steps involved in 2D separation protocol involving the pH-mediated on column sample stacking process: a) 1D gel electrophoresis separation; b) Transfer to 2nd dimension; c) Post-transfer on-column base stacking of sample band; d) 2D TGGE separation.

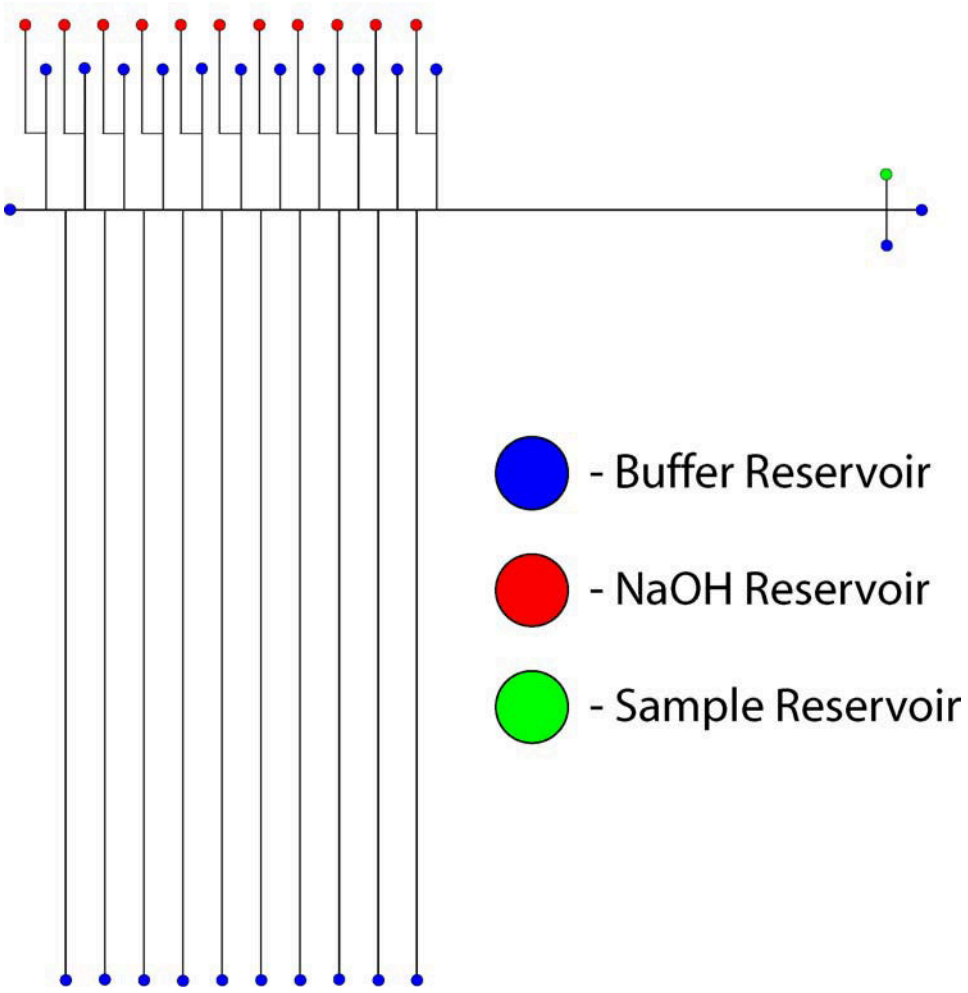

Figure 4.9 Design of modified 2D microfluidic network that allows for the employment of pH-mediated sample stacking technique following electrokinetic transfer of sample bands from first dimension to second dimension.

10 seconds, effectively stacking the transferred sample bands by the mechanism described above. The electric potential was returned to the buffer reservoirs and the parallel TGGE separation was commenced. Results from a 2D analysis of a heteroduplex mixture containing Mut_{100}, Mut_{200}, and Mut_{400} fragments are shown in Figure 4.10. Parallel TGGE was performed in the second dimension channels immediately following the base stacking process by externally generating a temporal thermal gradient by ramping the temperature from 69°C to 72°C over three minutes. The lower temperature range was required due to the use of lower ionic strength buffer in this case. From the results obtained, it is obvious that the separation efficiency and resolution of the heteroduplex samples are enhanced through incorporation on the sample band stacking process into the 2D separation protocol. An average ~1.8-fold increase in separation efficiency for the heteroduplex sample bands along with increased peak heights indicate effective sample stacking and concentration occurred following transfer of the bands into the second dimension channels.

CONCLUSION

The design of a parallel 2D microfluidic network with the potential for dramatically increasing the throughput of genetic mutation screening is proposed. The capability of the microfluidic system for performing comprehensive parallel 2D DNA separation is demonstrated through the analysis of simulated multiplex PCR products containing variation in both size and sequence. In the first separation

dimension, size variants within the injected sample band are segregated using standard gel electrophoresis. Following the first dimension separation, the size-

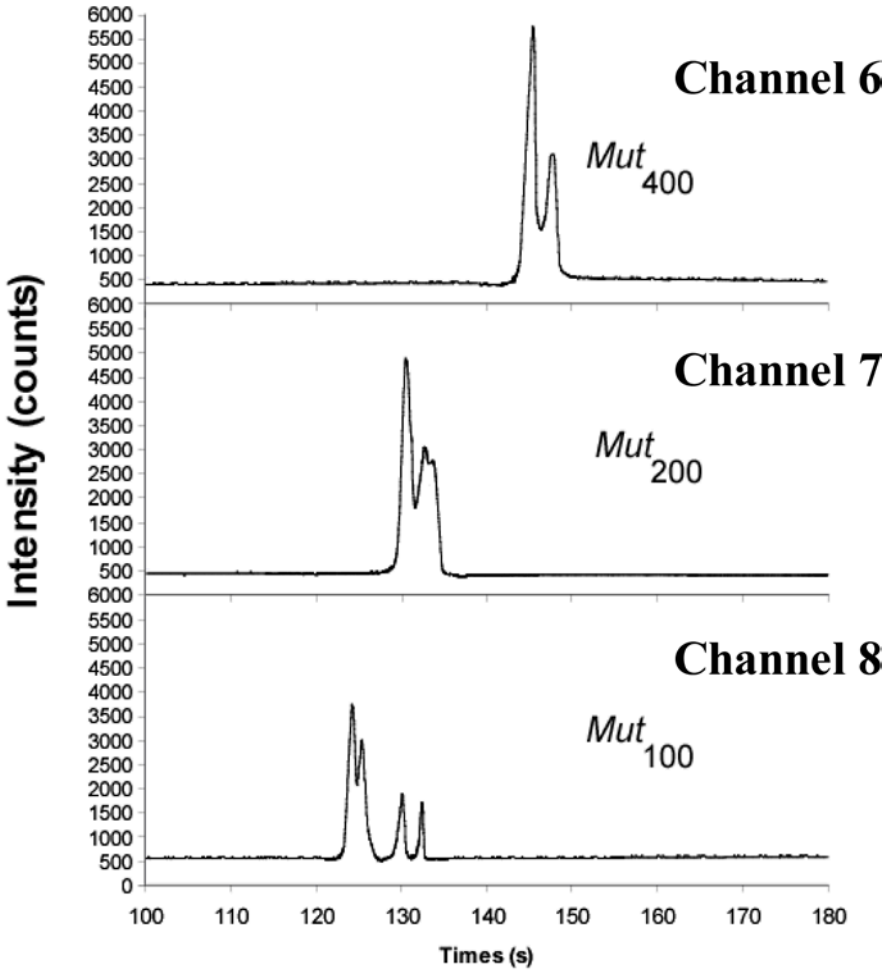

Figure 4.10 Electropherograms for comprehensive 2D DNA separation of heteroduplex samples consisting of a mixture of Mut_{100}, Mut_{200}, and Mut_{400} fragments. Separation efficiency and resolution are enhanced through incorporation of a sample band stacking process following the transfer of the bands into the second dimension and prior to commencement of the second dimension TGGE separation.

resolved DNA fragments are subsequently transferred to discrete second dimension channels where parallel, sequence-based TGGE separations are performed to interrogate each size variant for sequence heterogeneity using a temporal temperature gradient. Total analysis time is under 5 minutes.

Extensive finite element modeling determined that the 2D microfluidic network design could be further optimized by minimizing the widths of the interconnecting second dimension channels with respect to the width of the main first dimension separation channel. Optimization of the geometry factors involved in the network design are crucial in counteracting the sample band dispersion that is inherent in separation channels, such as the first dimension separation channel described here, which have discontinuous side walls. At present, the ratio of side channel width to main separation channel width used in the 2D channel network design is 0.4 with 40μm-wide second dimension channels representing the lower limit of our current microfluidic fabrication capabilities. Alternative fabrication methods must be explored to further improve the geometric optimization of the 2D microfluidic network design.

In addition to geometric optimizations, a chemical optimization of the system was demonstrated by the incorporation of a post-transfer sample band stacking method prior to the second dimension. Effectively performing this process is not trivial however, as the window in which it can be done is quite small. This is because it must be executed following the complete transfer of all bands into the second dimension to prevent re-broadening of the bands after stacking has already

been performed. Furthermore, the stacking must be carried out prior to the sample bands reaching the heated region of the second dimension channels. This is because stacking the band after commencing the TGGE separation will decrease the resolving power of the separation. Ultimately, however, the potential of parallel 2D microfluidic technology to rival and even supercede conventional mutation screening methods with a more automated, portable, and high throughput genomic technology is validated.

CHAPTER FIVE

SUMMARY AND CONCLUSION

The overall research objective of this project is to provide a higher throughput approach toward the screening of genomic DNA for sequence heterogeneity. This was to be achieved through the union of parallel multidimensional separation strategies with a microfluidic separation platform, in which the benefits of both can combine to achieve unparalleled throughput and analysis speed.

With the completion of the preliminary component of the Human Genome Project, the search for the role performed by specific genes and gene variants in disease has been greatly accelerated, especially for genes associated with cancer and genetic disorders. As the field of functional genomics advances, the identification of specific nucleotide variations, especially SNPs has become increasingly important in the attempt to increase present capabilities for detecting, monitoring and treating disease. Although nucleotide sequencing remains the prime means for identifying and characterizing sequence heterogeneity, the high costs and lengthy time expenditure associated with current sequencing technology makes alternative approaches more attractive in many cases. Furthermore, due to the low frequency

of mutations present in the genome (as noted previously), nucleotide sequencing by itself is an entirely inefficient approach to interrogating the entire genome. Thus, various methodologies have been developed to provide more cost-effective pre-screening of mutations in relatively large pieces of DNA. These methods primarily aim to screen through large amounts of DNA identify fragments of interest for further characterization by nucleotide sequencing or a specific assay. The work demonstrated here was aimed at developing a new, higher throughput mutation screening method by exploiting the advantages of microfluidic technology.

Initial work provided a foundation for micro-fabrication methods to be used later on. Specifically, a photolithographically-based methodology for fabricating microchannel structures on a silicon template master was developed and used to produce asters to be used in molding, imprinting, and embossing for the fabrication of microfluidic networks. The work described in Chapter 2 outlines a unique application to which these methods were directed.

The application of the field-effect for direct control of electroosmosis in a polydimethylsiloxane (PDMS)-based microfluidic system, constructed on a silicon wafer with a 2.0 μm electrically insulating layer of silicon dioxide, was demonstrated. This microfluidic system consists of a 2.0 cm open microchannel fabricated on a PDMS slab, which can reversibly adhere to the silicon wafer to form a hybrid microfluidic device. Aside from mechanically serving as a robust bottom substrate to seal the channel and support the microfluidic system, the silicon wafer is exploited to achieve field-effect flow control by grounding the semi-conductive

silicon medium. When an electric field is applied through the channel, a radial electric potential gradient is created across the silicon dioxide layer that allows for direct control of the zeta (ζ) potential and the resulting electroosmotic flow (EOF).

By configuring this microfluidic system with two power supplies at both ends of the microchannel, the applied electric potentials could be varied to allow for manipulation of the polarity and magnitude of the radial electric potential gradient across the silicon dioxide layer. At the same time, the longitudinal potential gradient through the microchannel, which is used to induce EOF, was held constant. The results of EOF control in this hybrid microfluidic system were presented for phosphate buffer at pH 3 and pH 5. EOF control was achieved at higher solution pHs of 6 and 7.4 by modifying the microchannel surface with cetyltrimethylammonium bromide (CTAB) was also presented. Finally, results of EOF control from this study were compared with those reported in the literature involving the use of fused-silica capillary systems and microfluidic devices under comparable conditions.

Chapter 3 outlines the efforts made to integrate a traditional mutation screening method, TGGE, onto a microfluidic platform. In this work, a miniaturized system for DNA mutation analysis, utilizing temperature gradient gel electrophoresis (TGGE) in a polycarbonate (PC) microfluidic device, was reported. By introducing a thermal denaturing gradient that results in differences of melting states for DNA samples of homogeneous size but heterogeneous sequence, the subsequent difference in average electrophoretic mobility allows TGGE to reveal

the presence of sequence heterogeneity in a given heteroduplex sample. Bulk heater assemblies were designed and employed to externally generate temperature gradients in spatial and temporal formats along the separation channels. TGGE analyses of model mutant DNA fragments, each containing a single base substitution, were achieved using both single and 10-channel parallel measurements in a microfluidic platform.

Additionally, a comprehensive polymer microfluidic device containing an integrated microheater and sensor array was developed and demonstrated for performing spatial TGGE for DNA mutation analysis. The device consisted of two PC modular substrates mechanically bonded together. One substrate was embossed with microchannels while the other contained a tapered microheater, lithographically patterned along with an array of temperature sensors. Compared with the external heating approaches, the integrated platform provided significant reduction in power requirement and thermal response time while establishing more accurate and highly effective control of the temperature gradient for achieving improved separation resolution.

Finally, Chapter 4 illustrates the realization of accomplishing a parallel two-dimensional separation in a microfluidic network to perform high throughput genetic mutation analysis of simulated multiplex PCR products. Geometric optimization of the microfluidic network design was investigated and implemented. Furthermore the separation process was enhanced through integration of a pH-mediated sample stacking technique following transfer of the sample bands from the

first dimension channel to the second dimension channels. These optimizations improved the overall efficiency and resolving power of the total system.

The comprehensive 2D mutation analysis performed with this platform demonstrated the ability to resolve a complex mixture and reveal sequence heterogeneity among target DNA fragments in approximately five minutes while maintaining adequate separation efficiencies. This reveals the potential of the system to provide tremendous improvement in analysis throughput over conventional technologies that require several hours to even days. Further enhancements of the facilities provided by this novel method will require alternative fabrication methods to silicon template embossing for fabrication of the microfluidic network that can allow for more advanced geometric optimization of the network design. Specifically, further reduction in the electric field non-uniformity along the length of the first dimension separation channel as well as an increase in the density of the second dimension microchannel array need to be addressed. Finally, the overall system needs to be fully automated into a self sufficient, autonomous platform to realize the reproducibility and sensitivity promised by this technology. This work will be essential for this method to approach the dependability and detection limits that are achieved by competitive mutation screening methods.

REFERENCES

1. Pauling, L; Itano, H. A.; Singer, S. J.; Wells, I. C. *Science* **1949**, *110*, 543-548.

2. Srivastava, S.; Zou, Z. Q.; Pirollo, K.; Blattner, W.; Chang, E. H. *Nature* **1990**, *348*, 747-749.

3. Eng, C., Vijg, J. *Nature Biotechnol***. 1997,** *15***,** 422-426.

4. Cohen, A. S., Najarian, D. R.; Paulus, A.; Guttman, A.; Smith, J. A.; Karger, B. L. *Proc. Natl. Acad. Sci. U.S.A.* **1987**, *85*, 9660-9663.

5. Smith, L. M. *Nature* **1991**, *349*, 812-813.

6. Fung, E. N.; Yeung, E. S. *Anal. Chem.* **1995**, *67*, 1913-1919.

7. Venter, J. C. et al. *Science* **2001,** *291*, 1304-1351.

8. Orita, M., Iwahana, H., Kanazawa, H., Hayashi, K., Sekiya, T., *Proc. Natl. Acad. Sci. USA* **1989**, *86*, 2766-2770.

9. Liu, Q., Sommer, S. S. *BioTechniques* **1995**, *18*, 470-477.

10. Southern, E. M. *Electrophoresis* **1995**, *16*, 1539-1542.

11. Chee, M. et al. *Science* **1996**, *274*, 610-614.

12. Winzeler, E. A. et al. *Science* **1998**, *281*, 1194-1197.

13. Fischer, S. G., Lerman, L. S. *Proc. Natl. Acad. Sci. USA* **1983** , *80*, 1579.

14. Sheffield, V. C., Cox, D. R., Lerman, L. S., Myers, R. M. *Proc. Natl. Acad. Sci. USA* **1989**, *86*, 232-236.

15. Abrams, E. S., Murdaugh, S. E., Lerman, L. S. *Genomics* **1990**, *7*, 463-475.

16. Gromp, M. *Nat. Genet.* **1993**, *5*, 111-117.

17. Fodor, S. P. A.; Read, J. L.; Pirrung, M. C.; Stryer, L.; Lu, A. T.; Solas, D. *Science* **1991**, *251*, 767-773.

18. Oefner, P. J.; Underhill, P. A. *Am. J. Hum. Genet.* **1995**, *57*, A266.

19. Fischer, S. G., Lerman, L. S. *Cell* **1979**, *16*, 191-200.

20. Barker, D. F. *Human Mut.* **2000**, *16*, 334-344.

21. J. Vijg *Biotechnology* **1995**, *13*, 137-139.

22. Vijg, J., van Orsouw, N. J. *Electrophoresis* **1999**, *20*, 1239-1249.

23. Wu, Y. et al. *Human Mut.* **1996**, *8*, 160-167.

24. van Orsouw, N.J. et al. *Hum. Mol. Genet.* **1996**, *5*, 755-761.

25. Nystrom-Lahti, M. et al. *Hum. Mol. Genet.* **1996**, *5*, 763-769.

26. Smith, W.M. et al. *Genet. Testing* **1998**, *2*, 43-53.

27. Rines, R.D. et al. *Carcinogenesis* **1998**, *19*, 979-984.

28. van Orsouw, N.J., Zhang, X., Wei, J.Y., Johns, D.R., Vijg, J., *Genomics* **1998**, *52*, 27-36.

29. Harrison, D. J., Manz, A., Fan, Z., Ludi, H., Widmer, H. M. *Anal. Chem.* **1992**, *64*, 1926-1932.

30. Harrison, D. J., Fluri, K., Seiler, K., Fan, Z., Effenhauser, C. S., Manz, A. *Science* **1993**, *261*, 895-897.

31. Chiem, N., Harrison, D. J. *Anal. Chem.* **1997**, *69*, 373-378.

32. Effenhauser, S. F., Manz, A., Widmer, H. M. *Anal. Chem.* **1993**, *65*, 2637-2642.

33. Effenhauser, C. S., Manz, A., Widmer, H. M. *Anal. Chem.* **1995**, *67*, 2284-2287.

34. Jacobson, S. C., Hergenroder, R., Koutny, L. B., Warmakc, R. J., Ramsey, J. M. *Anal. Chem.* **1994**, *66*, 1107-1113.

35. Woolley, A. T.; Mathies, R. A. *Anal. Chem.* **1995**, *67*, 3676-3680.

36. Schmalzing, D. et al. *Anal. Chem.* **1998**, *70*, 2303-2310.

37. Tian, H., Brody, L. C., Landers, J. P. *Genome Res.* **2000,** *10,* 1403-1413.

38. Tian, H., Jaquins-Gerstl A., Munro, N., Trucco, M., Brody, L. C., Landers, J. P. *Genomics* **2000**, *63*, 25-34.

39. Kopp, M. U.; de Mello, A. J.; Manz, A. *Science* **1998,** *280,* 1046-1048.

40. Waters, L. C.; Jacobsen, S. C.; Krotchinina, N.; Khandurina, J.; Foote, R. S.; Ramsey, J. M. *Anal. Chem.* **1998,** *70,* 158-162.

41. Weigl, B. H.; Yager, P. *Science* **1999,** *283,* 346-347.

42. Colyer, C. L.; Tang, T.; Chiem, N.; Harrison, D. J. *Electrophoresis* **1997,** *18,* 1733-1741.

43. Effenhauser, C. S.; Paulus, A.; Manz, A.; Widmer, H. M. Anal. Chem. **1994**, *66,* 2949-2953.

44. Woolley, A. T.; Lao, K.; Glazer, A. N.; Mathies, R. A. *Anal. Chem.* **1998,** *70,* 684-688.

45. Effenhauser, C. S.; Bruin, G. J. M.; Paulus, A. *Anal. Chem.* **1997,** *69,* 3451-3457.

46. Duffy, D. C.; McDonald, J. C.; Schueller, O. J. A.; Whitesides, G. M. *Anal. Chem.* **1998,** *70,* 4974-4984.

47. Martynova, L.; Locascio, L. E.; Gaitan, M.; Kramer, G. W.; Christensen, R. G.; MacCrehan, W. A. *Anal. Chem.* **1997,** *69,* 4783-4789.

48. Locascio, L. E.; Perso, C. E.; Lee, C. S. *J. Chromatogr. A* **1999,** *857,* 275-284.

49. Ocvirk, G.; Munroe, M.; Tang, T.; Oleschuk, R.; Westra, K.; Harrison, D. J. *Electrophoresis* **2000,** *21,* 107-115.

50. Soper, S. A.; Ford, S. M.; Qi, S.; McCarley, R. L.; Kelly, K.; Murphy, M. C. *Anal. Chem.* **2000,** *72,* 642A-651A.

51. Seiler, K.; Fan, Z. H.; Flurl, K.; Harrison, D. J. *Anal. Chem.* **1994,** *66,* 3485-3491.

52. Kovacs, G. T. A.; Petersen, K.; Albin, M. *Anal. Chem.* **1996**, *68,* 407A-416A.

53. Lee, C. S.; McManigill, D.; Wu, C. T.; Patel, B. *Anal. Chem.* **1991**, *63,* 1519-1523.

54. Ghowsi, K.; Gale, R. *J. Chromatogr.* **1991**, *559,* 95-101.

55. Hayes, M. A.; Ewing, A. G. *Anal. Chem.* **1992**, *64,* 512-516.

56. Poppe, H.; Cifuentes, A.; Kok, W. T. *Anal. Chem.* **1996,** *68,* 888-893.

57. Schasfoort, R. B. M.; Schlautmann, S.; Hendrikse, J.; van den Berg, A. *Science* **1999,** *286,* 942-945.

58. Polson, N. A.; Hayes, M. A. *Anal. Chem.* **2000,** *72,* 1088-1092.

59. Hayes, M. A.; Kheterpal, I.; Ewing, A. G. *Anal. Chem.* **1993**, *65,* 27-31.

60. Huang, T. L.; Tsai, P.; Wu, C. T.; Lee, C. S. A*nal. Chem.* **1993**, *65,* 2887-2893.

61. Huang, X.; Gordon, M. J.; Zare, R. N. *Anal. Chem.* **1988**, *60,* 1837-1838.

62. Barker, S. L.; Ross, D.; Tarlov, M. J.; Gaitan, M.; Locascio, L. E. *Anal. Chem.* **2000,** *72,* 5925-5929.

63. Highsmith, W. E., Jr.; Jin, Q.; Nataraj, A. J.; O'Connor, J. M.; Burland, V. D.; Baubonis, W. R.; Curtis, F. P.; Kusukawa, N.; Garner, M. M. *Electrophoresis* **1999**, *20*, 1186-1194.

64. Nataraj, A. J.; Olivos-Glander, I.; Kusukawa, N.; Highsmith, W. E., Jr. *Electrophoresis* **1999**, *20*, 1177-1185.

65. Henbenbrock, K.; Williams, P. M.; Karger, B. L. *Electrophoresis* **1995**, *16*, 1429-1436.

66. Thomas, G. A.; Williams, D. L.; Soper, S. A. *Clin. Chem.* **2001**, *47*, 1195-203.

67. Gelfi, C.; Righetti, S. C.; Zunino, F.; Della Torre, G.; Pierotti, M. A.; Righetti, P. G. *Electrophoresis* **1997**, *18*, 2921-2927.

68. Riesner, D.; Steger, G.; Zimmat, R.; Owens, R. A.; Wagonhofer, M.; Hillen, W.; Vollbach, S.; Henco, K. *Electrophoresis* **1989**, *10*, 377-389.

69. Gelfi, C.; Righetti, P. G.; Cremonesi, L.; Ferrari, M. *Electrophoresis* **1994**, *15*, 1506-1511.

70. Schell, J.; Wulfert, M.; Riesner, D. *Electrophoresis* **1999**, *20*, 2864-2869.

71. Gao, Q.; Yeung, E. S. *Anal. Chem.* **2000**, *72*, 2499-2506.

72. Kristensen, A. T.; Bjorheim, J.; Minarik, M.; Giercksky, K. E.; Ekstrom, P. O. *BioTechniques* **2002**, *33*, 650-653.

73. Zhu, L.; Lee, H. K.; Lin, B.; Yeung, E. S. *Electrophoresis* **2001**, *22*, 3683-3687.

74. Mao, H.; Holden, M. A.; You, M.; Cremer, P. S. *Anal. Chem.* **2002**, *74*, 5071-5075.

75. Steger, G. *Nucleic Acids Res.* **1994***, 22*, 2760-2768.

76. Ross, D.; Gaitan, M.; Locascio, L. E. *Anal. Chem.* **2001**, *73*, 4717-4123.

77. Mullis, K.; Faloona, F.; Scharf, S.; Saiki, R.; Horn, G.; Erlich, H. *Cold Spring Harbor Symp. Quant. Biol.* **1986**, *51*, 263-73. Rocklin, R. D.; Ramsey, R. S.; Ramsey, J. M. *Anal. Chem.* **2000**, *72*, 5244-5249.

79. Herr, A. E.; Molho, J. I.; Drouvalakis, K. A.; Mikkelsen, J. C.; Utz, P. J.; Santiago, J. G.; Kenny, T. W. *Anal. Chem.* **2003**, *75*, 1180-1187.

80. Chen, X.; Wu, H.; Mao, C.; Whitesides, G. M. *Anal. Chem.* **2002**, *74*, 1772-1778.

81. Nkodo, A.E.; Tinland, B. *Electrophoresis*. **2002,** *23*, 2755-65.

82. Ermakov, S. V.; Jacobson, S. C.; Ramsey, J. M. *Anal. Chem* **2000**, *72*, 3512-3517.

83. Jacobson, S. C.; Ermakov, S. V.; Ramsey, J. M. *Anal. Chem.* **1999***, 71,* 3273-3276.

84. Xiong, Y.; Park, S. R.; Swerdlow, H. *Anal. Chem* **1998**, *70*, 3605-3611.